

ESTIMATION OF MUSCLE ACTIVITY
USING PROBABILITY DENSITY FUNCTIONS
AND BAYES' THEOREM

by

Chad Vaughn Anderson

A Thesis Submitted to the Faculty of the
DEPARTMENT OF ELECTRICAL AND COMPUTER ENGINEERING

In Partial Fulfillment of the Requirements
For the Degree of

MASTER OF SCIENCE
WITH A MAJOR IN ELECTRICAL ENGINEERING

In the Graduate College

THE UNIVERSITY OF ARIZONA

2004

STATEMENT BY AUTHOR

This thesis has been submitted in partial fulfillment of requirements for an advanced degree at The University of Arizona and is deposited in the University Library to be made available to borrowers under rules of the Library.

Brief quotations from this thesis are allowable without special permission, provided that accurate acknowledgment of source is made. Requests for permission for extended quotation from or reproduction of this manuscript in whole or in part may be granted by the head of the major department or the Dean of the Graduate College when in his or her judgment the proposed use of the material is in the interests of scholarship. In all other instances, however, permission must be obtained from the author.

SIGNED: _____

APPROVAL BY THESIS DIRECTOR

This thesis has been approved on the date shown below:

_____	_____
Charles Higgins	Date
Assistant Professor of	
Electrical and Computer Engineering	

ACKNOWLEDGEMENTS

I would like to acknowledge Dr. Andrew Fuglevand who was instrumental in the formation and completion of this thesis. He provided laboratory facilities, equipment, funding, the guidance necessary to complete this thesis and worked with me as my research advisor. Thanks for all of your enthusiastic support Andy.

DEDICATION

I would like to dedicate this thesis to my wife Wendi and to my children Camden and Claire for all of their understanding, support, and help in completing this project. A special thanks to Wendi for her patience and the sacrifice willingly given during the last couple of years of research.

TABLE OF CONTENTS

Chapter 1: Introduction	8
1.1 Functional Electrical Stimulation.....	9
1.2 Analytical Biomechanical Models for Estimating Muscle Activity	10
1.3 Bayes' Theorem	10
1.4 Summary.....	11
Chapter 2: Data Collection	12
2.1 EMG Data Acquisition	12
2.2 Kinematic Data Acquisition.....	13
2.3 Procedures.....	14
Chapter 3: EMG Posterior Probability Density Function Estimation Using Bayes' Theorem.....	17
3.1 Discussion	17
3.2 Implementation and Computational Notes	19
Chapter 4: EMG and Kinematic Data Processing	21
4.1 Noise Reduction	21
4.2 High Frequency Noise	21
4.3 Low Frequency Noise.....	21
4.4 Muscle Activity.....	22
4.5 Finalizing and Normalizing	24
4.6 Preprocessing Kinematic Data	26
4.7 Extracting Position Data	27
4.8 Extracting Synchronization Data.....	27
4.9 Synchronizing Pulses from Data Acquisition Channel	28
4.10 Aligning the Kinematics into a Data Stream with a Consistent Time Base	28
4.11 Final Preprocessing Synchronized Kinematic Data	29
4.12 Estimating Probability Density Functions	29
4.13 Making a Prediction.....	32
4.14 Evaluating the Prediction.....	35
Chapter 5: Results	36
5.1 RMS Errors	38
Chapter 6: Discussion	43
6.1 For Future Study.....	44
6.2 Dimensionality	44
6.3 Independence Assumption	44
6.4 Kinematic Parameters.....	44
6.5 Implications for Functional Electrical Stimulation (FES).....	45
6.6 Summary	45
Appendix A – Atlas of Electromyography.....	47
References	57

LIST OF ILLUSTRATIONS

Figure 1: Overview of neuroprosthetic device.	8
Figure 2: The Experimental setup.	13
Figure 3: Overview of tasks 2 and 3.	15
Figure 6: Magnitude frequency response of noise reducing band pass filter.	22
Figure 7: Envelope showing approximation of actual whole muscle activity or muscle force as compared to recorded EMG.	23
Figure 8: Magnitude frequency response of low pass filter.	24
Figure 9: Example comparison of raw recorded EMG and estimated muscle activity.	25
Figure 10: Data flow path of kinematic pre-processing.	26
Figure 11: Extracting the joint probabilities.	30
Figure 12: Example joint probability density function.	31
Figure 13: Example resulting array of joint density functions.	32
Figure 14: Demonstration of how a prediction is formed.	33
Figure 15: Example one dimensional sample histograms.	35
Figure 16: Overlay of positions during 10 trials of task 4 (squares.	36
Figure 17: The Repeatability of predictions.	37
Figure 18: Tasks ranked in order of ascending RMS error.	40
Figure 19: Muscles ranked in order of ascending RMS error.	42
Figure 20: The location of M1, serratus anterior.	47
Figure 21: The location of M2, anterior deltoid.	48
Figure 22: The location of M3, posterior deltoid.	48
Figure 23: The location of M4, pectoralis major.	49
Figure 24: The location of M5, latissimus dorsi.	49
Figure 25: The location of M6, teres major.	50
Figure 26: The location of M7, biceps brachii.	51
Figure 27: The location of M8, brachialis.	52
Figure 28: The location of M9, brachioradialis.	53
Figure 29: The location of M10, triceps.	54
Figure 30: The location of M11, extensor carpi radialis.	55
Figure 31: The location of M12, flexor carpi radialis.	56

LIST OF TABLES

Table 1: Names of the 12 muscles used in this experiment and their primary functions. 12	
Table 2: Synopsis of RMS errors collapsed over all muscles.	39
Table 3: Synopsis of muscle RMS errors collapsed over all tasks and trials.	41

ABSTRACT

Towards the development of a neuroprosthetic system through which paralyzed individuals with C5 or C6 spinal chord injuries regain full functional control of their limbs, a means of estimating muscle activity level from desired kinematic values is required. This thesis presents a method of performing this estimation. It uses *a priori* distribution functions and Bayes' theorem to find the *a posteriori* distribution of possible muscle activity levels given a specified set of kinematic values. The *a priori* distribution functions were estimated with data taken during a training task. The system was tested by comparing predicted to actual muscle activity levels during seven different tasks, none of which was used in establishing the *a priori* distribution functions. The system worked well with the overall RMS error of 6.1% across all muscles and all tasks.

Chapter 1: Introduction

For more than 20 years, physiologists have been working to improve the quality of life for paralyzed individuals through the use of functional electrical stimulation which involves artificial stimulation of muscles in order to produce limb movement. Today, the best systems are still extremely limited in their ability to produce natural movement. Functional electrical stimulation has the potential to be of great benefit to paralyzed individuals if the control interface can be made flexible enough to facilitate production of a wide repertoire of movements.

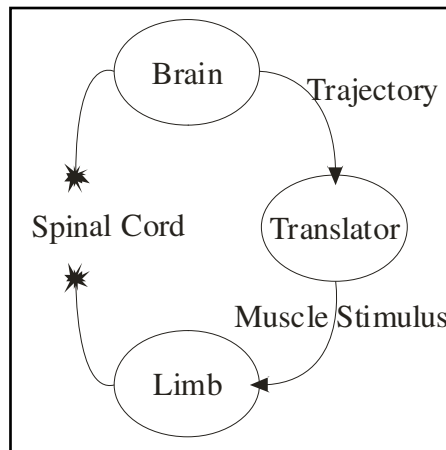


Figure 1: Overview of neuroprosthetic device.

In pursuit of a neuroprosthetic system wherein paralyzed individuals with C5 or C6 spinal chord injuries (paralyzed from the neck down) regain control of their limbs, a translator device must be devised that is capable of producing muscle-activity signals from trajectory related signals (Figure 1). However, due to the complex mechanics of the human limb associated with its many degrees of freedom and its redundant, non-linear actuators, operating according to an as yet undetermined control law, it is unlikely that linear controllers will soon be capable of controlling the system. The complex interactions among these characteristics suggest that the use of non-deterministic, or at least non-linear, methods might be the only way to achieve satisfactory control of a human arm. One solution might be achieved through the use of probabilistic methods. This project presents a non-deterministic controller in the form of a probabilistic predictor of muscle activity patterns based on Bayes' Theorem.

Recently, neuroscience researchers have made significant progress in distilling trajectory information from the activity of neural populations in the motor cortex and other areas of the brain[6]. For example, Nicolelis and colleagues [14], [23], and

Schwartz and colleagues [22] have shown that trajectory information can be extracted from the activity of a sampled population of neurons in the motor cortex which appear to be directionally tuned. Then, using this population vector as the desired trajectory, they have produced a system which allows a monkey to control a robotic arm to perform various tasks. However, few attempts have been made to distill muscle activity information from the brain in the same manner.

1.1 Functional Electrical Stimulation

Functional electrical stimulation (FES) is a process wherein muscles are stimulated artificially via implanted or surface electrodes rather than by nerves delivering internally generated signals. FES has been used to augment the movement capabilities of people who have, through injury to the spinal chord, lost some or all of their ability to control the movement of their limbs [7], [8] and hands [17], [18].

In an ideal FES system, a wide range of desired trajectories could be readily transformed into the appropriate patterns of muscle stimulations needed to evoke the corresponding natural movements. These movements would in turn closely track the desired trajectory.

Currently, FES systems are far from realizing this ideal. There are two main versions of FES systems used by paralyzed patients. In one system, desired EMG signals for specific movement sequences are recorded from an able-bodied subject and stored in digital format. Then, when triggered by the patient (often through some type of voice recognition system), those signals are “replayed” through a set of stimulators to drive the muscles to reproduce the expected movement [8]. This approach is limited because only the specific movements which have been prerecorded can be used. In this system, the entire movement sequence is replayed upon triggering and cannot be modified prior to or during execution so as to achieve a trajectory other than the one recorded. The second deployed type of FES system is used by paralyzed patients that have retained some voluntary control of trunk and/or limb muscles. The EMG produced by these muscles is used to drive an FES controller. While these systems are generally used to augment retained movement [19], they have also been used to restore lost movement [7]. In both versions of current FES systems, the primary limitation is that muscle stimulation patterns cannot be readily estimated for a desired movement variation. This lack of a generalized translation scheme has limited the usefulness of such systems. Consequently, researchers have considered several approaches for producing a more generalized FES controller. First, research has been primarily focused on the use of biomechanical models [17]. Given a good model, the relationship between kinematics and muscle activity can be found and used to solve the EMG estimation problem. More recently, a few attempts at using artificial neural networks have been used to find similar kinematic parameter to

muscle activity mappings [1], [4], [13]. This project presents a third approach, which is to relate kinematic parameters and muscle activity through a probabilistic mapping.

1.2 Analytical Biomechanical Models for Estimating Muscle Activity

In theory, the most direct way of obtaining good estimations of muscle activity would be to reverse engineer the system, breaking it down into a set of actuators and levers which behave in a predictable fashion. Since about 1980, physiologists and engineers have approached the problem of estimating muscle force, which is monotonically related to muscle activity estimated from electromyographic (EMG) recordings, from a traditional Newtonian mechanics perspective [17], [21]. The general approach taken has been to calculate the torques at each joint, given the masses and kinematics of the limb segments. Next, by introducing some knowledge of where muscles attach to the bony segments, lever arms and joint moments were found. Then, applying knowledge about contractile properties of muscle, force and associated muscle activity for some group of muscles was estimated for the kinematics of the limb [20], [21]. There are several problems, however, with this inverse dynamics approach to the estimation of muscle activity. Because the characterization of the contractile and mechanical properties of a muscle, its end connections, and other details are still incompletely understood, there are many assumptions and estimations that go into such a model [20]. These estimations form a primary source of error built into the model itself. Additionally, real joints do not operate as simple pivot joints, the distribution of mass of limb segments is not uniform or linear, and multiple joints are linked together giving rise to complex interactions. Even if these complex features of a limb could be accurately modeled, and all assumptions and estimations made were accurate, then muscle redundancy and multiple degrees of freedom still result in an ill-posed problem which can only be solved by applying additional system constraints such as optimal control laws. However, researchers have still not come to an agreement as to what kinds of optimal control laws are best for use in a generalized system which controls the movement of a human limb [17]. Therefore, the use of inverse dynamics based on biomechanical models has not been used successfully as a general purpose control strategy in FES systems.

1.3 Bayes' Theorem

In a departure from the biomechanical model to predict or estimate muscle activity for use in an FES system, this thesis presents a statistical predictor based on probabilistic relationships between kinematic information and muscle activity. The statistical predictor used is based on Bayes' Theorem which is a tool used to find the probability of the occurrence of some event given the prior occurrence of some other event (Chapter 3). It has been employed in many ill-posed inverse problems and sensor fusion type tasks [9], [11], [2].

From a more biological standpoint, Zhang and colleagues [26] successfully used Bayes' Theorem to infer the position of a rat's head in a 64×64 cm grid based on the patterns of spiking activity from simultaneously recorded hippocampal place cells as the rat wandered around an arena. They found relative mean errors of 2-3 cm between the predicted and actual positions. They also reported that the theoretical minimal error was also between 2 and 3. This was significantly better than estimations of position based on population vector and basis function approaches.

The Bayesian approach was applied to a specific case of medical diagnosis by Blinowska and colleagues [2] as part of a larger expert system. They attempted to differentiate the cause of hypertension between essential hypertension and five types of secondary causes given general patient information, such as blood pressures, clinical symptoms, and biochemical test results. Their goal was to obtain at least 70% correct decisions within each cause of hypertension. They correctly diagnosed the malady between 66% and 92% correct depending on which of the 6 causes of hypertension was investigated.

Bayes' theorem was used by Seifert and Fuglevand [18] to predict patterns of muscle activity in three muscles, an extensor and two flexors, which controlled the three primary joints of the finger, the metacarpalphalangeal, the proximal interphalangeal and the distal interphalangeal joints, given joint-angle trajectory data. Then, stimulus pulse trains derived from predicted muscle activity levels were delivered to muscles in an attempt to evoke desired movements. This system produced acceptable errors ($12.1 \pm 3.2\%$ RMS error) when comparing the predicted patterns of muscle activity to actual recorded EMG patterns for the same task. This system also produced acceptable errors (16.7% mean RMS error) when comparing the desired finger movements to the finger movements produced by the artificial stimulus pattern.

1.4 Summary

This thesis extends the work done previously by Seifert and Fuglevand by showing that Bayes' theorem can be used to estimate the activities of many muscles associated with complex natural movements of the human arm from trajectory information.

Chapter 2: Data Collection

EMG signals were recorded from 12 muscles (Table 1) using bipolar surface mounted silver-silverchloride electrodes with diameters of 4 mm. and inter-electrode spacing of approximately 2 cm.

Muscle Name	Primary Muscle Function
Serratus Anterior	Protracts shoulder by rotating the scapula in an upward fashion.
Anterior Deltoid	Draws arm forward (shoulder flexion).
Posterior Deltoid	Draws arm backwards (shoulder extension).
Pectoralis Major	Flexes, adducts, and medially rotates humerus.
Latissimus Dorsi	Extends, adducts, and medially rotates humerus.
Teres Major	Laterally rotates humerus.
Biceps Brachii	Flexes elbow, supinates forearm and flexes shoulder.
Brachialis	Flexes elbow.
Brachioradialis	Flexes elbow.
Triceps Brachii	Extends elbow.
Extensor Carpi Radialis Longus	Extends and adducts wrist.
Flexor Carpi Radialis	Flexes and abducts wrist.

Table 1: Names of the 12 muscles used in this experiment and their primary functions.

The silver-silverchloride electrodes were chosen because they are very stable electrically and widely used for surface EMG recording. This electrical stability significantly reduces noise artifact arising from the deformation of the skin under the electrode [5]. The locations of the EMG electrodes for each of the 12 muscles are shown in appendix A.

2.1 EMG Data Acquisition

EMG signals were differentially amplified by 1000 and band-pass filtered (-6 dB. cutoff points at 100 Hz and 1000 Hz) by a bank of 12 analog Grass amplifiers, model 12A5. The low cutoff was chosen to help remove 60 Hz noise and movement artifact, most of which fell between 0 and 100 Hz as determined by experimentation. It should be noted that the analog filters had a slow roll off, approximately -6 dB per decade, so that signals required further (digital) filtering as part of the preprocessing step.

Next, EMG signals were sampled and digitized by a Cambridge Electronic Design Ltd. Power 1401 data acquisition system. The sample rate was 2000 samples per second per channel. After amplification, EMG amplitudes were on the order of ± 0.1 V. Analog data were digitized with 16-bit range mapping to ± 5 V, for a precision of $152 \mu\text{V}$ or approximately 1350 levels within the EMG amplitude range.

The EMG data acquisition setup described here is the same as the setup used by Seifert and Fuglevand [18].

2.2 Kinematic Data Acquisition

For this experiment, the kinematic data parameters of interest were the horizontal, x , and vertical, y , positions of the endpoints of the various limb segments in a 2-D plane. Five markers were positioned to identify endpoints of body segments including the hip, shoulder, elbow, wrist, and hand (metacarpal phalangeal joint on the ulnar aspect of the hand) (Figure 2). Each marker consisted of a cotton swab dipped in glow-in-the-dark paint and mounted in a small plastic fixture. Experiments were conducted in low light conditions and the position of each marker was recorded by a single camera on digital video.

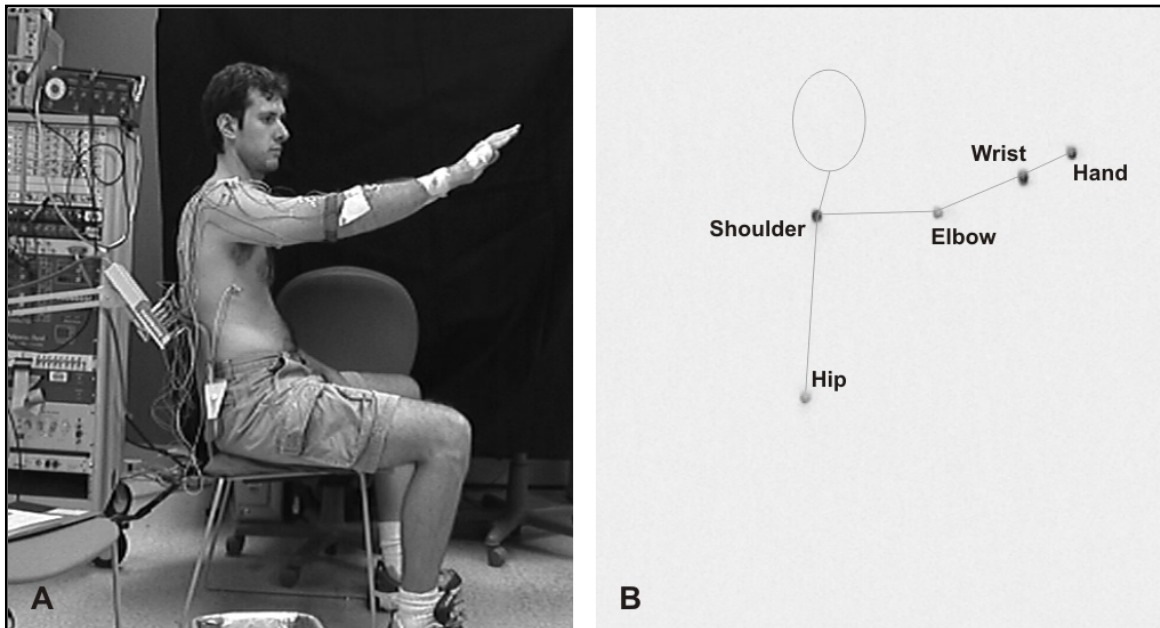


Figure 2: The Experimental setup. **A)** Subject in normal light conditions, sitting in chair, ready to begin experiment. **B)** Subject in low light conditions, sitting in chair, ready to begin experiment. Markers showing positions are glowing and appear as dots. (Text labels and stick figure have been added for clarification.)

In addition to the position of each marker, the digital video also recorded an LED as it flashed on and off which served as a synchronization mechanism. A driving pulse turned on the LED for 1/20 second which was guaranteed to be long enough to be captured on at least one video frame. The LED was then switched off for the remaining 19/20 of that second. The driving pulse which turned on the LED was also recorded by the same data acquisition system that acquired the EMG data and was the key element in synchronizing the kinematic data to the EMG data.

2.3 Procedures

For task one, the subject was first asked to move his arm throughout the sagittal plane (the plane perpendicular to the floor and running front to back) in a random fashion. The subject was instructed to generate a variety of movements at varying speeds and to try to move through every point in the two-dimensional workspace without flexing the trunk. Furthermore, the subject was asked to focus on making natural movements without excessive muscle co-contraction. This task was performed for 15-20 minutes while EMG and kinematic data were recorded. These data were used to establish the *a priori* probability density functions used in the Bayes' theorem predictor.

The subject was then asked to perform seven specific movement tasks. The subject was asked to move at a natural speed and to repeat each task at least ten times keeping velocity and position characteristics as consistent as possible across trials of a task. The subject paused for 1 – 2 sec. between trials of a task.

For tasks two and three (Figure 3), the subject was instructed to start from a resting position with the arm pendent, raise the arm to about eye level, then trace out a side-ways figure eight, or infinity symbol, with the hand beginning the movement up and forward from the center of the symbol (task two) or beginning the movement down and towards the body (task three). After completing the motion, the subject returned the arm to the resting position. The completion of these steps formed a single trial. The subject was asked to complete at least ten trials for each task.

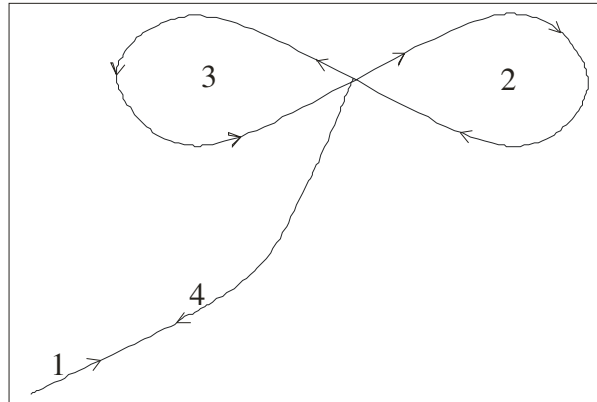


Figure 3: Overview of tasks 2 and 3. In task 2, the subject was asked to trace out a sideways figure eight, or an infinity pattern, in the forward direction. **1)** Beginning at rest, raise arm to eye level. **2)** Trace first lobe of infinity pattern. **3)** Trace second lobe of infinity pattern. **4)** Lower hand to resting position. In task 3, the subject reversed steps 2 and 3.

For tasks four and five (Figure 4), the subject was instructed to start from a resting position, raise their arm to mid-chest level, then, beginning at the bottom corner closest to themselves, to trace out a figure of a square. Initial direction of the movement was in the outward (or upward during the fourth task) direction. After returning to the starting corner, the subject was to return his or her arm to the resting position. The completion of these steps formed a single trial. The subject was asked to complete at least ten trials for each task.

For tasks six, seven, and eight (Figure 5), the subject was instructed to start from a rest position, reach out as if pressing a button located at the extent of their reach at head, shoulder or knee height respectively, and then return the hand to the rest position. The completion of a single reach formed a single trial. The subject was asked to complete at least ten trials for each of these tasks.

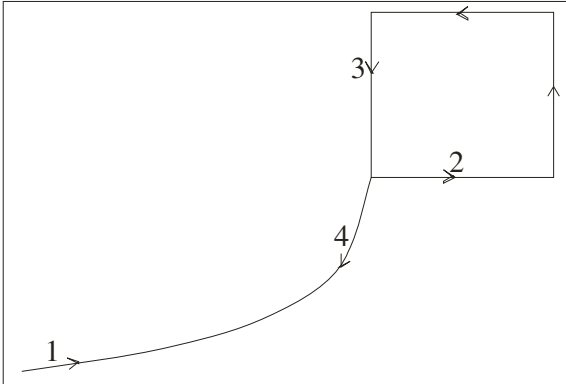


Figure 4: Overview of tasks 4 and 5. In task 4, the subject was asked to trace out square pattern in the forward direction. **1)** Beginning at rest, raise arm to shoulder level. **2)** Trace first side of square. **3)** Trace last side of square. **4)** Lower hand to resting position. In task 5, the subject reversed steps 2 and 3.

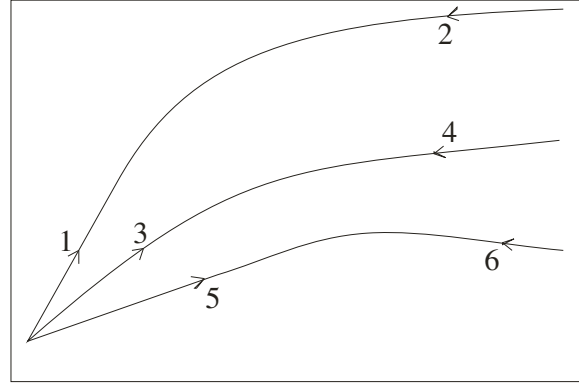


Figure 5: Overview of tasks 6 – 8. In task 6, the subject was asked to reach to head level. **1)** Beginning at rest, reach to head level. **2)** Lower arm to the resting position. In task 7, the subject reached to shoulder level **3)** Beginning at rest, reach to shoulder level. **4)** Lower arm to the resting position. In task 8, the subject reached to knee level **5)** Beginning at rest, reach to the knee level. **6)** Return arm to the resting position.

Chapter 3: EMG Posterior Probability Density Function Estimation

Using Bayes' Theorem

Bayes' theorem is a statistical tool by which the posterior probability of the occurrence of an event A , given that event B has already occurred, can be found even when it cannot be measured or calculated directly. The power of Bayes' theorem is that it constitutes an indirect path for obtaining otherwise unobtainable conditional probabilities [2]. Its power is geometrically expanded when used in conjunction with the law of total probability. The law of total probability allows Bayes' theorem to be used to find the probability of the occurrence of event A given that events B , C , D , and so on, have already occurred.

3.1 Discussion

Bayes' theorem is generally most useful when used in conjunction with the relation of conditional probabilities shown in equation 1.

$$P(A|B) = \frac{P(B|A) \cdot P(A)}{P(B)} \quad 1$$

$P(A|B)$ is the *a posteriori* probability of the occurrence of event A given that event B has occurred, $P(A)$ is the *a priori* probability of the occurrence of event A , $P(B)$ is the *a priori* probability of the occurrence of event B and $P(B|A)$ is the probability of the occurrence of event B given that event A has already occurred. For use in this project, the general form was modified in the following manner.

Since the probability of event B given the prior occurrence of event A , multiplied by the probability of the occurrence of event A is equal to the joint probability of the event A and B , the following relation can be formed (Equation 2).

$$P(B|A) \cdot P(A) = P(B, A) \quad 2$$

Then, by combining equations 1 and 2 the following relation can be formed.

$$P(A|B) = \frac{P(A,B)}{P(B)} \quad 3$$

To find its final form, Bayes' theorem is applied to the conditional probability relation shown in equation 3.

$$P(A|B) = \frac{P(A,B)}{\sum_A P(B|A) \times P(A)} \quad 4$$

The denominator in equation 4 serves as a normalization factor. The summation over all values in the domain of A ensures that the histogram resulting from finding $P(A|B)$ sums to unity. It also normalizes with respect to the probability density function of A , in case $P(A)$ wasn't uniformly distributed across the possible range so that each bin in the probability density function $P(A|B)$ is equally weighted.

For the experiment, the general result from equation 4 must be expanded because the parameter of interest is dependent on the occurrence of not a single event, B , but several events, e.g. B , C , and D . The expansion of equation 4 is shown in equation 5.

$$P(A|B,C,D) = \frac{P(A,B,C,D)}{\sum_A P(B|A) \cdot P(A) \times \sum_A P(C|A) \cdot P(A) \times \sum_A P(D|A) \cdot P(A)} \quad 5$$

Equation 5 presents a problem. Even when the values of the events A , B , C and D are limited to a small range, a huge number of samples would be needed to find a reasonable estimate of the joint probability, $P(A,B,C,D)$. To make the problem more tractable, a reduction in dimensionality is necessary. This reduction is achieved by assuming that events B , C , and D are independent and then applying the law of total probability to the independent conditional probabilities. The result is described in equation 6.

$$P(A|B,C,D) = P(A|B) \times P(A|C) \times P(A|D) \quad 6$$

The combination of equations 4 and 6 results in equation 7 which then simplifies to the final, usable, form given in equation 8.

$$P(A|B,C,D) = \frac{P(A,B)}{\sum_A P(B|A) \cdot P(A)} \times \frac{P(A,C)}{\sum_A P(C|A) \cdot P(A)} \times \frac{P(A,D)}{\sum_A P(D|A) \cdot P(A)} \quad 7$$

$$P(A|B,C,D) = \frac{P(A,B) \cdot P(A,C) \cdot P(A,D)}{\sum_A P(B|A) \cdot P(C|A) \cdot P(D|A) \cdot P(A)^3} \quad 8$$

Though estimating $P(A,B)$, $P(A,C)$, and $P(A,D)$, is still difficult, each of these estimations require many fewer samples than $P(A,B,C,D)$. Furthermore, $P(A)$ is an *a priori* quantity as are the conditional probabilities, $P(B|A)$, $P(C|A)$, and $P(D|A)$.

3.2 Implementation and Computational Notes

Restating equation 7 once more with A , B , C , and D replaced with descriptions specific to this experiment gives the implemented form of the conditional probability relation of equation 1 combined with Bayes' theorem.

$$P(EMG_{M1} | (X,Y)_{elbow}, (X,Y)_{wrist}, \dots) = \frac{P(X_{elbow}, EMG_{M1})}{\sum_{EMG1} P(X_{elbow} | EMG_{M1}) \cdot P(EMG_{M1})} \times \frac{P(Y_{elbow}, EMG_{M1})}{\sum_{EMG1} P(Y_{elbow} | EMG_{M1}) \cdot P(EMG_{M1})} \times \dots \quad 9$$

In equation 9, the ordered pairs $(X,Y)_{xxx}$ are the positions of the respective markers and EMG_{Mx} , represent the muscle activity of a specific muscle, Mx . The predicted muscle

activity level is defined to be the expected value of the probability density function which is found when equation 9 is evaluated for each level of muscle activity.

Equation 9 was developed previously by Seifert and Fuglevand [18]. Its derivation is given here for completeness.

Though Seifert and Fuglevand made use of joint angle velocities in their investigation of the Bayesian prediction technique [18], preliminary studies, done in conjunction with the work in this thesis, showed that no improvement was achieved through the addition of velocity or acceleration factors. This finding was contrary to expectation and should receive a more complete investigation.

The joint probability density functions, e.g. $P(X_{hand} | EMG_{M1})$, and the probability density function of the muscle activity, e.g. $P(EMG_{M1})$, for each muscle can be pre-computed from the data gathered during the random movement task (task 1, see page 17). These density functions remain useful as long as the correlations between muscle activity and kinematic value don't change with the passage of time or between data sets. Having determined the joint densities and the overall EMG density, the conditional probability density function from which predictions are formed can be easily determined. This was the approach taken in this study.

To predict the level of muscle activity in one muscle at a single time increment required the evaluation of the quantity on the right side of equation 9. When the probability density functions are binned in one percent increments, as they were in this project, estimating the muscle activity at a specific time, t , involved $2 * n * 100$ multiply operations and 100 divide operations where n was the number of kinematic parameters considered. For this project there were six kinematic parameters (x and y coordinates for elbow, wrist, and hand). Therefore, for each time bin, a prediction was formed for 12 muscles from six kinematic parameters requiring approximately 14,400 multiply operations and 1,200 divide operations. Each time bin was approximately 33 ms. Even general purpose micro-processors have no trouble performing this number of operations in less than the duration of one time bin and thus, this system could be easily be deployed to a real time framework.

Chapter 4: EMG and Kinematic Data Processing

The file containing recorded EMG data was opened in Matlab and read and the 16-bit ADC data was converted to double precision floating point format. The remaining preprocessing was significant and included a noise reduction step, a muscle modeling step, and a finalization/normalization step.

4.1 Noise Reduction

Visual inspection of the raw recorded EMG signals and analysis of the temporal frequency power spectra showed two types of noise present in our signal. Large amplitude spikes constituted the first type of noise. The source of these spikes is unclear though cable movement artifact is suspected. The second type of noise was relatively low frequency noise. In a separate set of pilot experiments, it was observed that cable movement artifact was the primary source of this second type of noise.

4.2 High Frequency Noise

High frequency noise present in the recorded EMG signals appeared as large amplitude spikes. Amplitudes of these spikes were significantly larger than the amplitudes of recorded EMG signals. They were large enough to distort the normalized EMG thereby degrading the Bayesian predictor's performance. In an effort to reduce the effect of these large amplitude spikes, the following heuristic was implemented. For each channel, the DC bias was first removed by subtracting the mean of the recorded EMG signal. Then, in an iterative procedure, a threshold was found which threshold was the amplitude level below which 99.99% of the data points fell. All data points with amplitude values above this threshold, namely <0.01% of the total number of data points, were clipped to the threshold value. Visual inspection of the EMG showed that this method was effective in removing large-amplitude high-frequency noise spikes (Figure 9, page 31).

4.3 Low Frequency Noise

In a separate set of studies, power spectra of EMG signals recorded during static muscle contractions with no cable movement were computed. The bandwidth of the surface detected EMG under these conditions was approximately 60 to 500 Hz. EMG signals recorded while the muscles were at rest, but with imposed cable movement, fell into the 0 to 300 Hz range and had significantly more total power than the EMG signals during the static contractions did. For the two muscles investigated in this set of studies, the signal to noise ratio was -38.57 dB and -22.28 dB. In an effort to boost the signal to noise ratio, an aggressive zero phase digital band pass filter was applied. The filter was a

20th order Butterworth with a passband frequency range of 100 to 500 Hz. (Figure 6). This aggressive band pass filter was applied in addition to the filtering done by the analog amplifiers and was necessary because of the slow rolloff characteristics of the amplifiers' built in filters. A Butterworth type filter was chosen to comply with normally accepted practices for EMG processing by physiologists [24]. The passband frequency cutoffs were chosen as a compromise level between low frequency noise and signal. The filter cutoffs did result in slight attenuation of the signal, but they also severely attenuated the main part of the noise. In the set of mini-experiments conducted, the attenuation of the total signal power was small, 0.2 dB (2%) and 0.3 dB (3%) for each of the two muscles respectively. On the other hand, much of the noise was removed. The total power of the noise was reduced by 17.3 dB (86%) and 17.7 dB (87%) on each of the respective channels. This boosted the overall signal to noise ratio by over 17 dB (700%) on each channel.

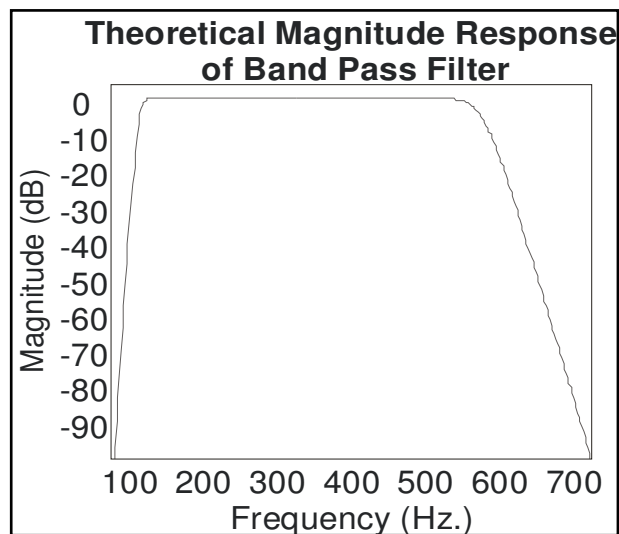


Figure 6: Theoretical magnitude frequency response of noise reducing band pass filter.

4.4 Muscle Activity

Surface recorded EMG signals are the summation of the electrical activity of muscle fibers near the recording site. The electrical activity recorded is the spike-like variation of the voltage potential across a muscle fiber's cell membrane due to the arrival of an action potential [10]. These EMG signals range over positive and negative values and range in frequency from about 10 Hz to 500 Hz [24].

The signal of interest, however, is not EMG but the tensile force of the entire muscle developed at its end points. Surface recorded EMG signals bear little

resemblance to the activity of the contractile apparatus which underlies the development of tensile force by skeletal muscle. Unlike EMG, muscle force is unidirectional; it does not have both positive and negative amplitude components. Muscle activity ranges in frequency from approximately 0 Hz to 5 Hz [10]. Muscle activity is the instantaneous summation of all the muscle fiber activity across the whole muscle and can be thought of as the envelope containing the positive portion of the EMG [10] (Figure 7).

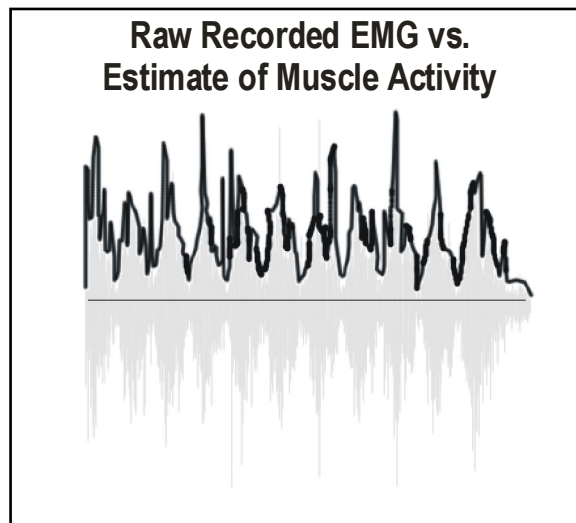


Figure 7: The muscle activity or muscle force may be thought of as the positive envelope (thick black line) containing the recorded EMG (gray trace).

The relationship between recorded EMG and muscle activity described previously suggests a processing method for approximating muscle activity from recorded EMG. First, the EMG is rectified to produce a unidirectional signal. Second, the recorded EMG is low pass filtered with a 6 Hz cutoff. In this experiment, a 6th order Butterworth zero phase low pass filter with -3 dB point at 6 Hz (Figure 8) was used. The resulting signal is an estimate of muscle activity and will be referred to as such.

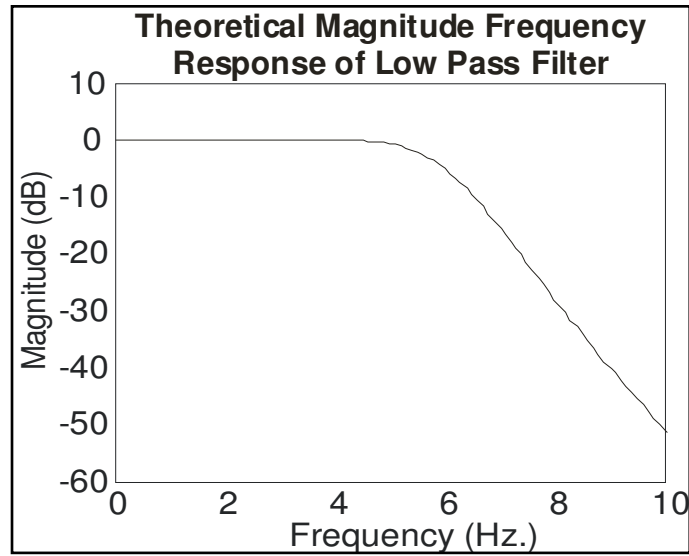


Figure 8: Theoretical magnitude frequency response of low pass filter.

4.5 Finalizing and Normalizing

The band-limited estimate of muscle activity was downsampled from 2000 Hz to 30 Hz for alignment to the kinematic data. Finally, the amplitude was normalized to the range 0.0 to 1.0, and the ends were trimmed to remove the transients introduced during filtering (Figure 9).

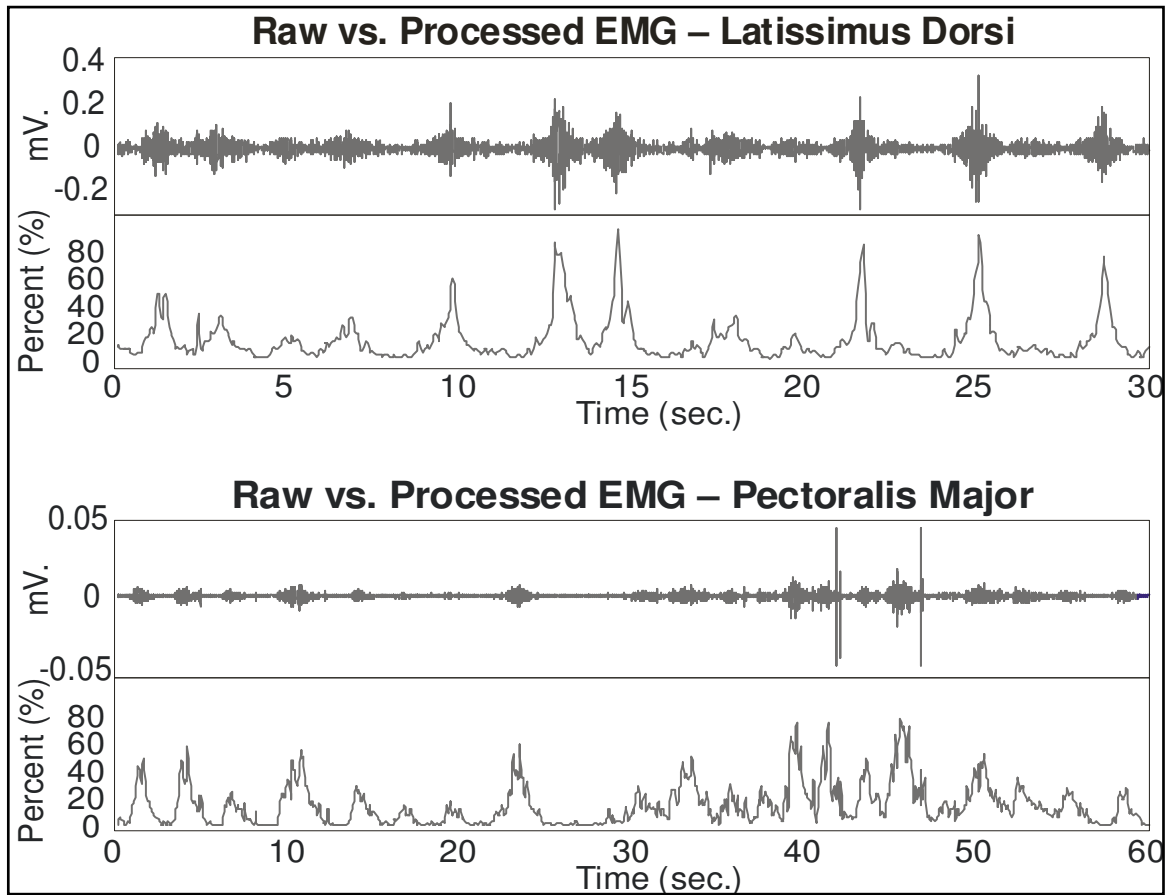


Figure 9: Example comparison of raw recorded EMG and estimated muscle activity for two muscles, Latissimus Dorsi and Pectoralis Major. Data was taken from task 1, the random movement task. Note the removal of spikes in the EMG recording of the Pectoralis Major. Also, note the scaling to 100% on both muscles from their baseline levels.

4.6 Preprocessing Kinematic Data

Kinematic data were recorded optically with a digital video recorder. It was important to maintain proper alignment between the kinematic data and the recorded EMG data over the entire time course of the experiment in order to ensure that the joint probability density functions which characterized the statistical relationship between muscle activity and kinematics at the beginning of the experiment also characterized their statistical relationship at the end of the experiment. The danger was that if errors due to dropped or added frames were allowed to propagate through the data, the delays

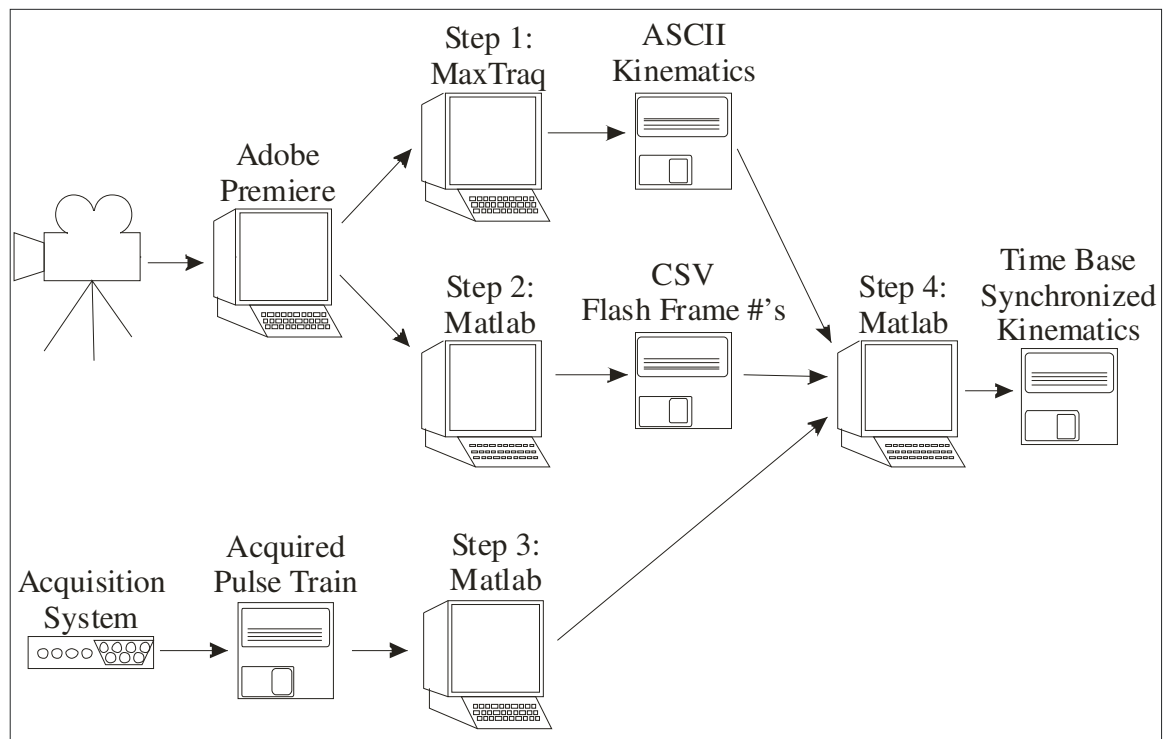


Figure 10: Data flow path of kinematic pre-processing showing first four of five steps. **Step 1)** Extract the kinematic position information from recorded video. **Step 2)** Extract the frame numbers from frames with LED pulses for synchronization. **Step 3)** Extract time bins of edges of synchronizing pulses from data acquisition channel. **Step 4)** Combine into a time base synchronized data stream filled with kinematic data.

introduced could become significant. For this, reason great care was taken to align the kinematic data and the recorded EMG data and every effort was taken to minimize phase distortion. The kinematic data preprocessing can be broken down into five steps, extracting the position data from the video, extracting the frame numbers of synchronizing frames containing the LED flash, extracting synchronization time bins

from the recorded synchronizing pulses, combining kinematic data and synchronizing pulses into a time base synchronized data stream, and final preprocessing (Figure 10).

4.7 Extracting Position Data

The first step in preprocessing the kinematic data was to transfer the digital video captured during the experiment to a computer using the Adobe Premiere video editing package. It was then recompressed to the Intel Indeo 5 codec and exported to a Microsoft .avi file. This file was then opened by the MaxTraQ software package for digitization and tracking. After being processed by MaxTraQ, an ASCII file containing header information and the (x,y) position in pixels of the position markers during each frame was generated. This file was the basis for subsequent analysis. (Figure 10, step 1)

4.8 Extracting Synchronization Data

For the second kinematic preprocessing step, the Microsoft .avi file generated by Adobe Premiere was searched for the number of each frame wherein the synchronizing LED flash was visible. To determine if a frame should be marked as a synchronizing frame, RGB data from each frame were summed to yield a composite image of the frame's activity. Next, the area of the frame within which the LED flash appeared was searched. If the activity level exceeded a threshold, that frame was flagged as a synchronizing frame and the frame number was stored. If more than one consecutive frame was found to exceed threshold level then each frame of the sequence was compared and the frame number of the frame with the maximum activity level was stored. The threshold was set by manually tracking the activity level of the region of interest over several cycles of the flashing LED. After processing the entire file, the frame numbers of the synchronizing frames were written to a file as a comma separated vector (Figure 10, step 2).

While the digital video captured was nominally 30 frames per second, the actual sample rate was 29.97 frames per second, the NTSC standard. This meant that on occasion, there would be 29 frames per second. Additionally, the possibility of a dropped frame also would result in 29 frames per second. These occurrences were rare but occurred often enough to cause significant relative phase distortion between muscle activity and kinematic signals if uncorrected. Additional complicating factors included the unknown frame transition gap and the exposure time which lead to the occasional occurrence of a second containing 31 frames. It was critical for the kinematic and EMG data to be properly aligned in time so the occasional second containing fewer than or more than 30 frames created a potential problem which compounded for long experiments. To ensure that these inconsistencies in the frame capture did not adversely affect the predictor's performance by causing the signal statistics to change with time, the

kinematic data were realigned at each one second interval so that epochs containing only 29 frames were padded to 30 frames and any epochs containing 31 frames were clipped. The collection of one second intervals each with 30 data points was then pieced together to form a single kinematic data set with a consistent time base and was ready to be aligned to the synchronizing pulse train recorded by the data acquisition system along with the EMG.

4.9 Synchronizing Pulses from Data Acquisition Channel

The third step towards synchronizing the recorded EMG and the kinematic data was to process the synchronizing pulse channel. This channel was acquired by the same data acquisition system as the EMG signals and so it was already aligned in time with the recorded EMG. The channel contained a series of square wave pulses, one for each pulse of the LED, and was obtained by recording the output which drove the LED on an acquisition channel. To find the rising edges, the square pulses on this channel were first downsampled from 2000 Hz to 30 Hz to match the video capture rate. This had the effect of compressing the square pulse which drove the LED into an impulse type signal. The downsampled signal was then differentiated. A threshold was used to find the rising edges and the number of edges found was counted. This number was compared to the number of flashes recorded by the camera and stored in the comma-separated vector mentioned previously. A discrepancy between the number of synchronizing video frames and the number of recorded synchronizing pulses indicated that there was a problem somewhere in the process. Either the threshold in finding the rising edges of the pulses was wrong and an edge had been missed, the video processing had not found an existing synchronizing flash of the LED, or there was an error during the experiment wherein the data acquisition machine began flashing the synchronizing light before the camera began to acquire video (Figure 10, step 3).

4.10 Aligning the Kinematics into a Data Stream with a Consistent Time Base

When the two numbers matched, alignment could be done without introducing any estimations or approximations. In addition to finding the number of rising edges, the time bin of each rising edge was found. The frame containing the flash of the LED could be aligned to the time bin containing the rising edge and plateau. This was done by beginning at a reference frame and aligning all the raw data from the reference frame back to the previous reference frame. In this way the data was always exactly aligned to the EMG data at at least one point during each second. At this point, the raw kinematic position data generated by the MaxTraq software had been inserted into a time base aligned vector and was ready for further processing (Figure 10, step 4).

4.11 Final Preprocessing of Synchronized Kinematic Data

The fifth step in the preprocessing of the kinematic data was a filtering and normalizing step. The synchronized data was smoothed by applying the same low pass Butterworth filter used for the EMG data, -3 dB at 6 Hz (Figure 8). The 6 Hz cutoff frequency was chosen for the same reason it was used to filter the EMG during its preprocessing. Kinematic position data were then normalized to a scale of 0.0 to 1.0 where zero mapped to one edge of the camera's range of view and one mapped to the other edge. This global scaling was used, instead of scaling to maximal displacement, in order to keep consistent scaling between trials and tasks.

The experiment did not include muscles that control the movement of the trunk of the body. Therefore, the sites of interest, the elbow, the wrist, and the hand, were all measured relative to the shoulder position. Though small (maximum displacement of the shoulder marker from the mean was between 2% and 8% in the y direction and 4% and 6% in the x direction depending on task), there was some trunk movement during the tasks. To remove these effects, the mean of all the recorded shoulder marker positions was found. Then, for each frame the deviation of the shoulder marker position from the mean shoulder marker position was found and subtracted from the elbow position, wrist position, and hand position during that frame. This resulted in elbow, wrist and hand positions relative to a fixed shoulder position.

4.12 Estimating Probability Density Functions

Once the kinematic and EMG data were processed and aligned, two important statistical measures were computed from the task 1 data. The overall density function of muscle activity for each muscle throughout the entire task was found first. The normalized amplitude range, 0.0 to 1.0, was binned by percent and included 0% and 100% (101 bins total). For each muscle, a histogram of the amplitudes was computed. The bin counts were normalized to sum to unity and the result was treated as the sample probability density function of the muscle activity. The amplitude probability density function was used in the Bayes' process to normalize the conditional probability densities (Equation 9).

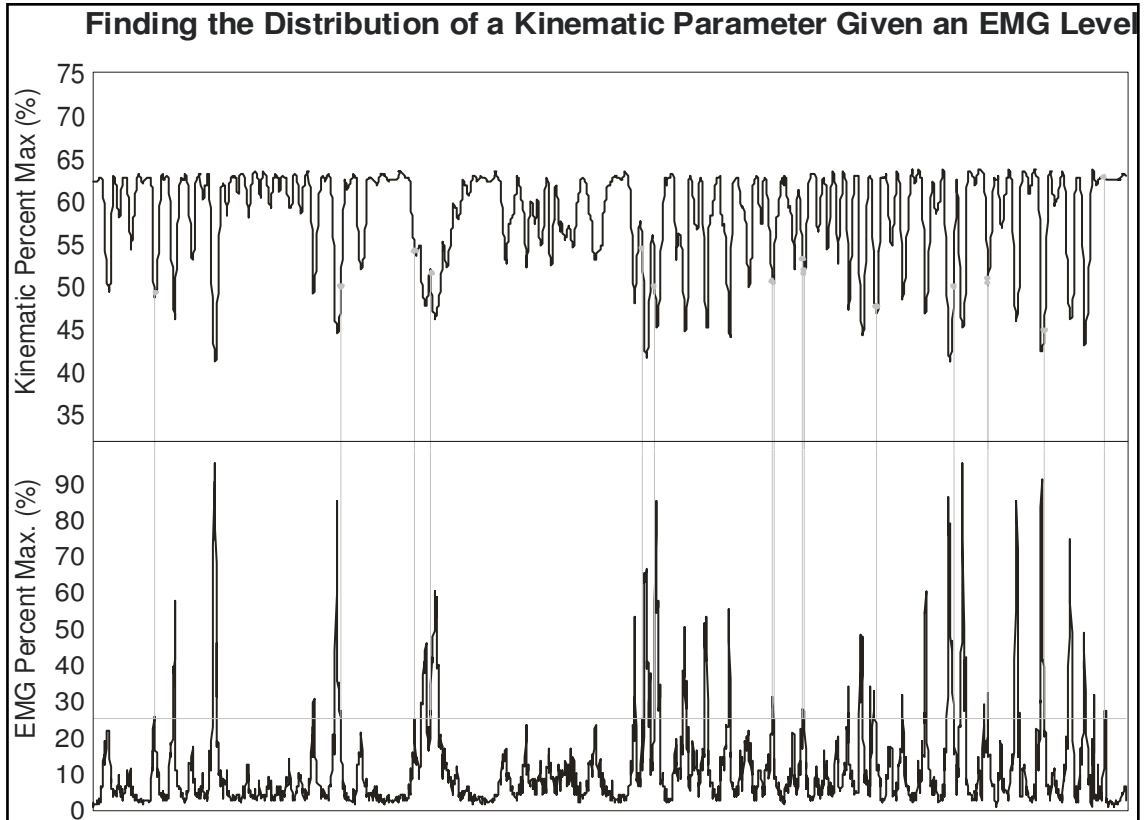


Figure 11: Extracting the probability density function for a kinematic parameter associated with one level of muscle activity. For a level of muscle activity (25% shown here), the corresponding list of kinematic parameter values is found and those bins are incremented. An estimate of the joint probability density function results from performing this process for each level of muscle activity.

According to equation 9, the other parameter of interest is the joint statistics. The joint probability density function between each muscle and each kinematic parameter was found in the following manner. For each level of muscle activity, 0% - 100%, a histogram was made from the corresponding values of a kinematic parameter (Figure 11). When normalized, the array of histograms formed the sample joint probability density function (Figure 12). After forming the sample joint probability density functions for each (muscle, kinematic parameter) pair, they are combined into a multidimensional array containing joint probability density functions (Figure 13).

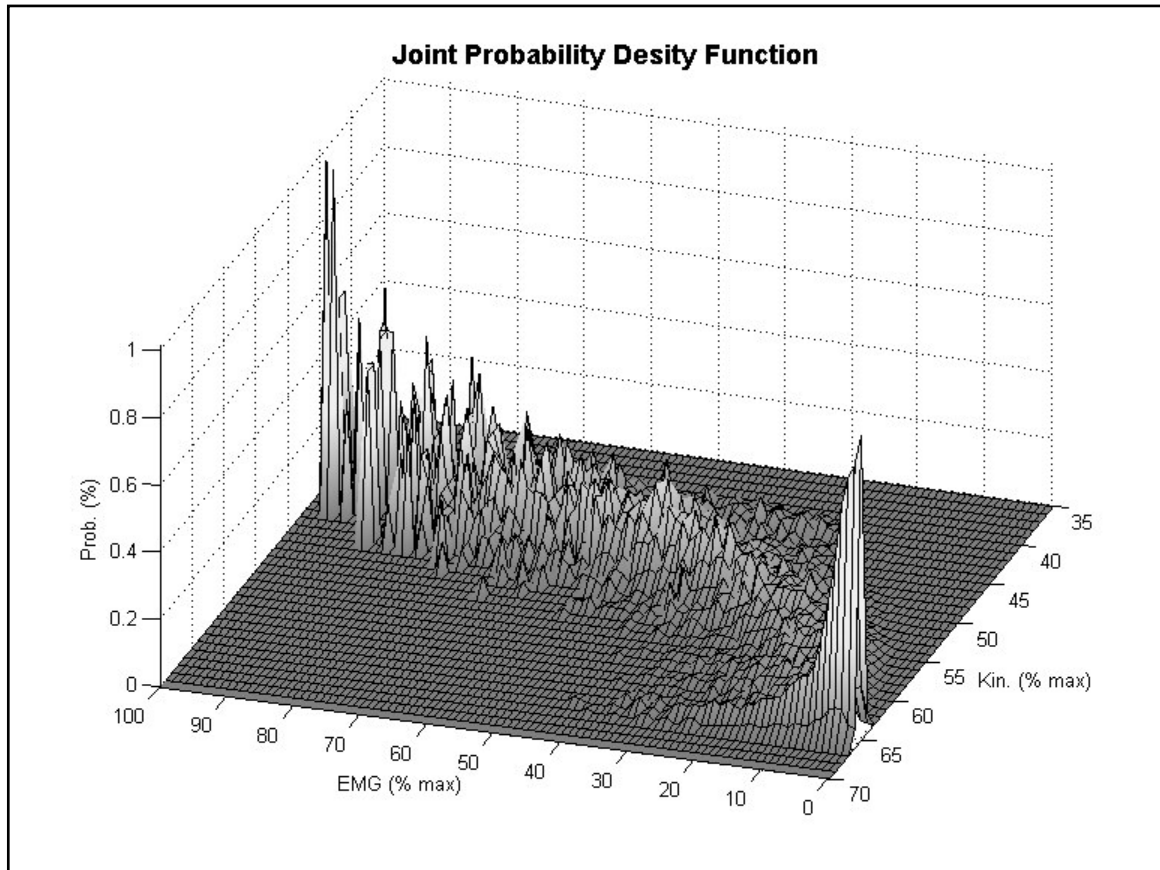


Figure 12: Example joint probability density function.

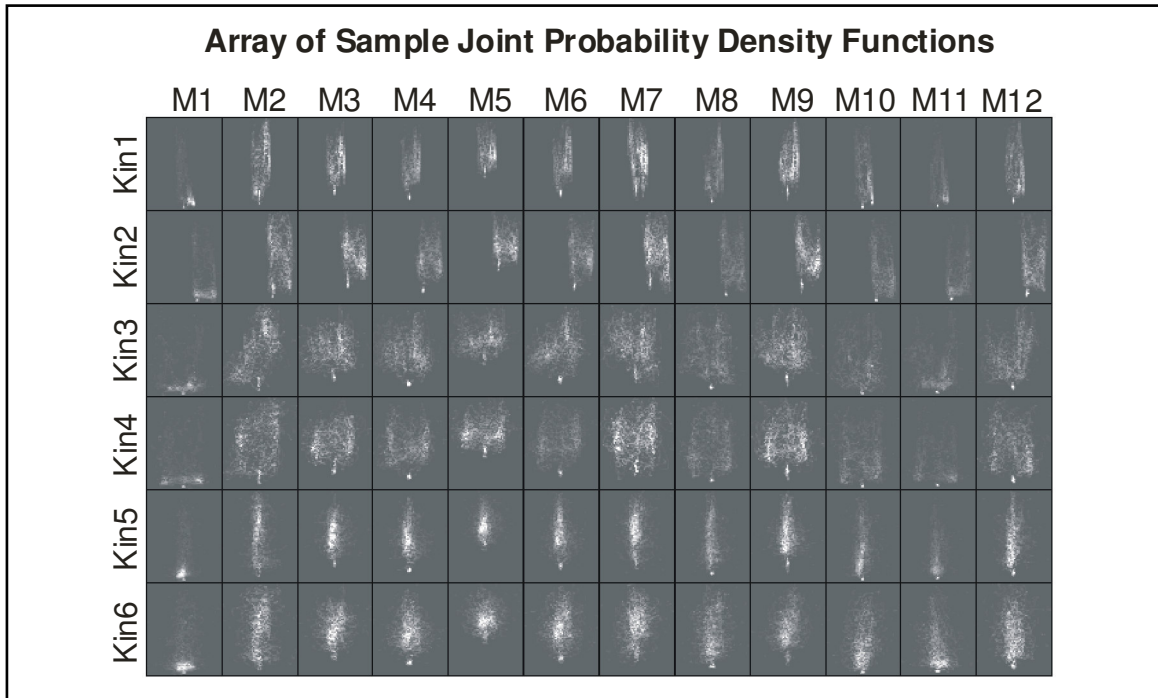


Figure 13: Example resulting array of joint density functions. Each muscle e.g. M1 or M7, and kinematic parameter e.g. position, velocity, pair has an associated joint probability density function which maps the relationship between the muscle activity values and kinematic values. Each bin in the array shown here contains a joint probability density function shown as a contour map).

4.13 Making a Prediction

Making a prediction involved five steps. First, the given muscle and kinematic parameters were used as indices for finding the desired joint probability density function. Second, for the given value of each kinematic parameter of interest, a histogram was selected from the joint distribution function (Figure 14.a, 14.b, and 14.c). Third, each was normalized according to Bayes' theorem (Equation 9 and Figure 14.d). This method of normalization was important in this experiment because the joint probability density function represents the joint statistics of a non-uniform data set, i.e. the muscle

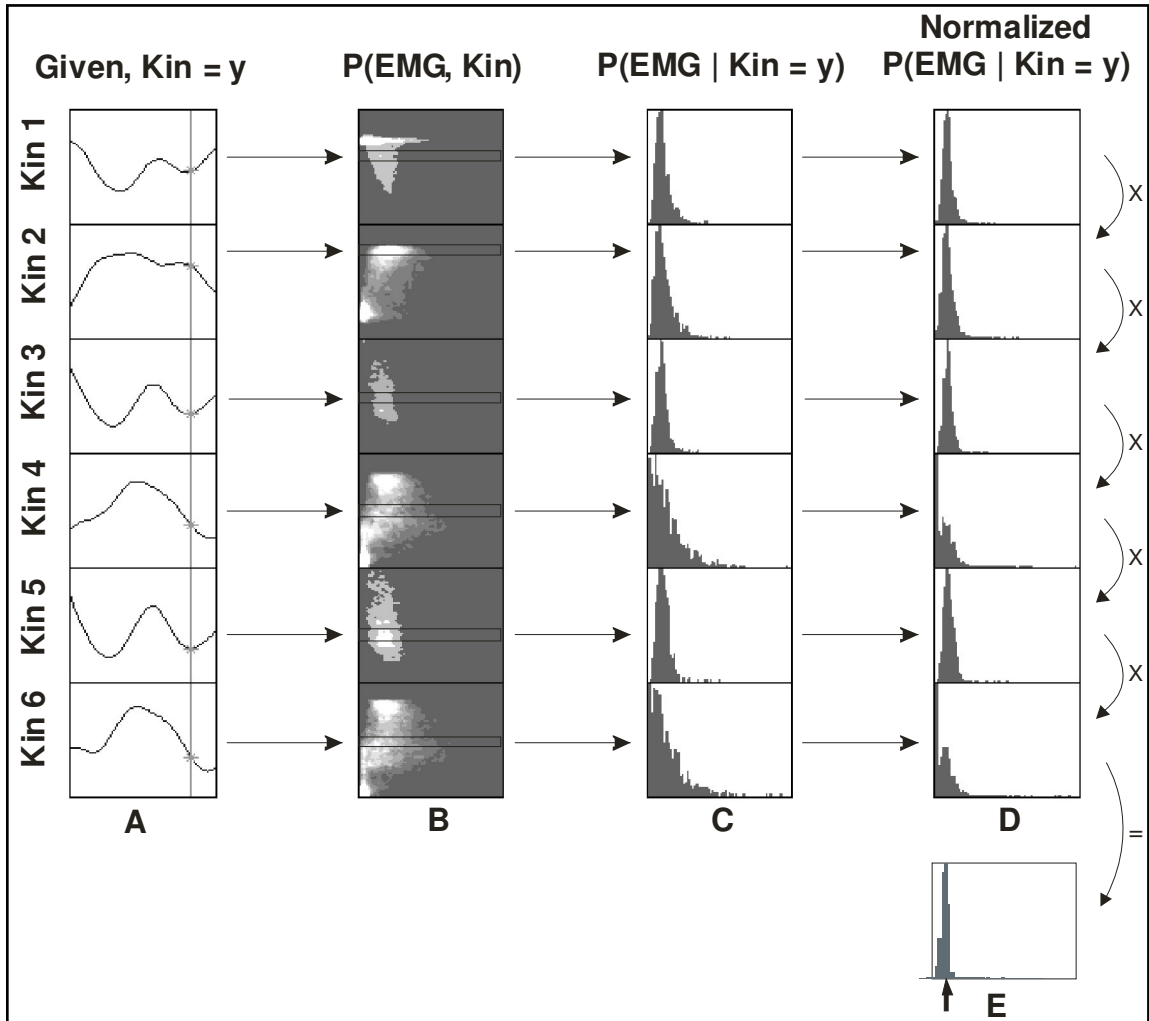


Figure 14: Demonstration of how a prediction is formed. **A)** Given a set of desired kinematic parameters, select the value at time = t . **B)** Use the values selected in A as indices into appropriate joint probability density functions. **C)** Retrieve the indexed histogram. **D)** Normalize by density of muscle activity for the given muscle and multiply all resulting histograms together. **E)** The final probability density function and the expected value (arrow) which becomes the predicted muscle activity value.

activity values were small more often than they were large. The non-uniformity of the sample data skews the joint probability density function and this normalization corrects for that factor. Fourth, corresponding elements from each of the normalized probability density functions were multiplied together according to the Law of Total Probability (Figure 14.e). The product histogram was then renormalized such that it summed to unity and was defined to be the resultant probability density function. Fifth, a prediction of the muscle activity for each particular muscle, given the specific kinematic combination, was found by calculating the expected value of the resultant probability density function (Figure 14.e).

As an example, suppose it is desired to predict the muscle activity of the pectoralis major, given that the y position of the elbow is 75%. First, select the joint probability density function which associates M4 with Kin2 (Figure 13). Next, select the histograms for the given kinematic values of 75% (Figure 15). Once these histograms have been normalized, the expected value can be found and a prediction made (Figure 14).

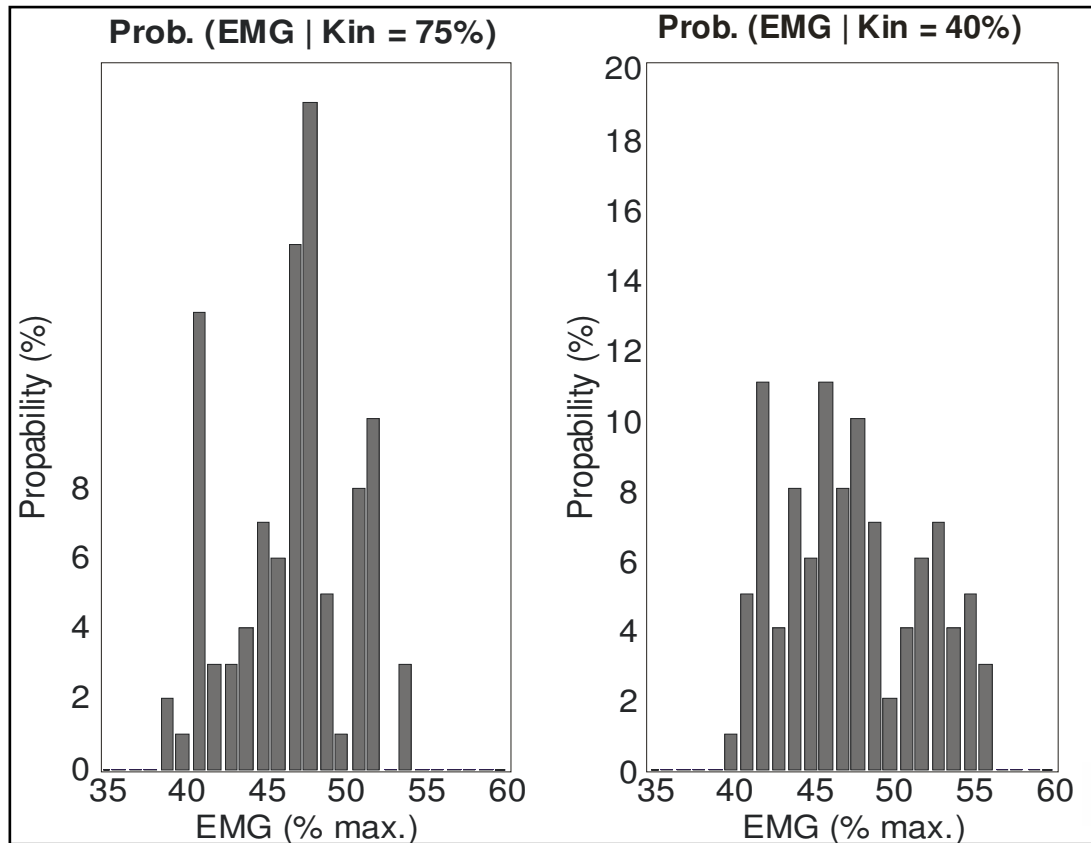


Figure 15: Example one dimensional sample histograms of estimated muscle activity, given two different levels of kinematics, 75% and 40%.

4.14 Evaluating the Prediction

Evaluation of the prediction was made by finding the RMS error between the predicted values of muscle activity and its actual values.

Chapter 5: Results

Figure 16 shows an example of the trajectories of the elbow, wrist and hand during repeated trials of task 4. Slight variations in limb trajectory during successive trials probably contributed to the variation in the detected muscle activity across trials.

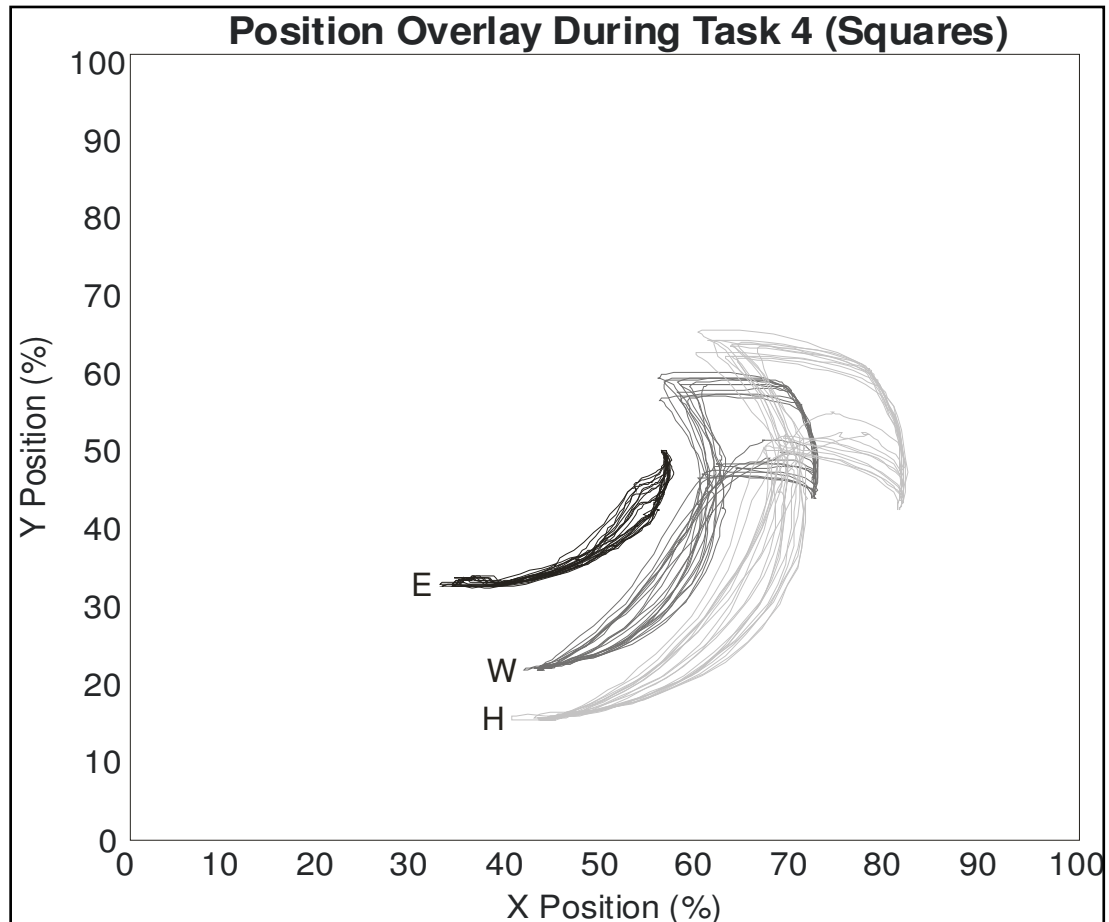


Figure 16: Overlay of positions during 10 trials of task 4 (squares). **E** shows the path of the elbow marker. **W** shows the path of the wrist marker and **H** shows the path of the hand marker. Note the slight variation in position for repeated trials which lead to small variations in muscle activity during repeated trials.

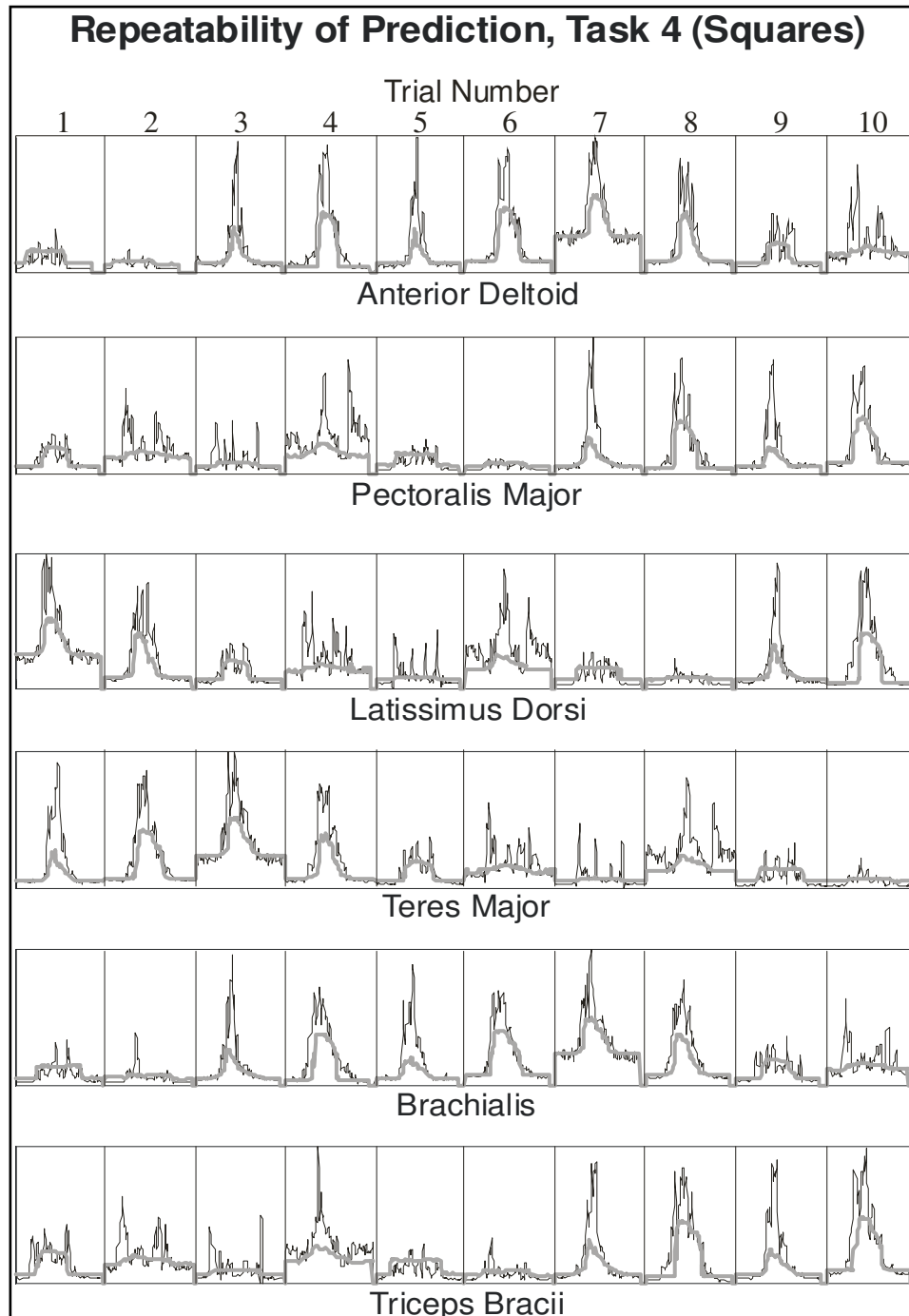


Figure 17: The Repeatability of predictions. For 10 trials of task 4, the desired (actual) muscle activity (shown as the thin black line) and the predicted muscle activity (shown as the thick gray line) are overlaid. Note the variation in desired muscle activity on repeated trials. Also note the good correspondence between the predicted and the desired even with the variation of desired muscle activity during repeated trials of the same task.

Figure 17 shows the desired and predicted muscle activity during task 4 (squares task). Note the variation in the desired muscle activity for repeated trials of the same task within the same muscle. This variation in muscle activity is expected and most likely arises from slight variations in limb trajectory. Despite these variations, the Bayes' method of predicting muscle activity from kinematics yielded good estimates of muscle activity on a trial-to-trial basis.

5.1 RMS Errors

Overall, the RMS error for all muscles and tasks was small with a mean (\pm SD) of $6.11 \pm 3.06\%$ (range 1.03% to 17.37%). Table 2 shows the RMS errors according to task. The best predicted tasks were task 7 (the midlevel reach), task 8 (the low level reach) and task 2 (the forward direction figure eights). The data of table 2 are summarized in figure 18.

Movement Task	Mean RMS Error % ± Standard of Deviation	Min. / Max. RMS Error %
Task 2 - Figure Eights (forward)	6.24 ± 3.18	1.24 / 17.37
Task 3 - Figure Eights (reverse)	5.36 ± 2.20	1.45 / 10.03
Task 4 - Squares (forward)	4.73 ± 1.82	1.38 / 8.16
Task 5 - Squares (reverse)	6.29 ± 2.49	1.22 / 11.86
Task 6 - High Reach	7.93 ± 3.93	1.40 / 16.49
Task 7 - Midlevel Reach	3.72 ± 1.65	1.03 / 7.49
Task 8 - Low Reach	4.03 ± 2.16	1.06 / 8.83
Overall	6.11 ± 3.06	1.03 / 17.37

Table 2: Synopsis of RMS errors collapsed over all muscles. Values given in percent.

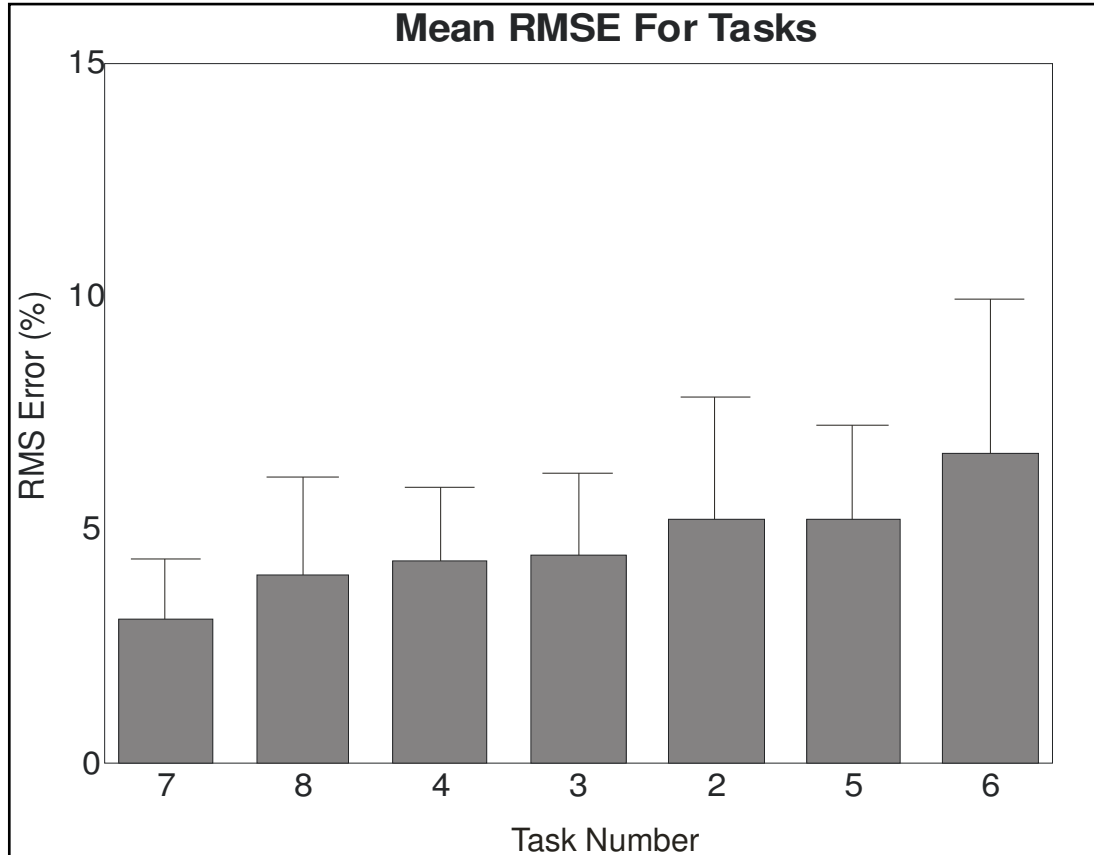


Figure 18: Tasks ranked in order of ascending RMS error.

Table 3 shows the RMS errors for each muscle across all tasks. Figure 19 shows the mean (\pm SD) for each muscle ranked in ascending order according to RMS error. M12, flexor carpi radialis, and M11, extensor carpi radialis longus, were the best predicted muscles (Figure 19). Though, for the tasks studied, these muscles showed little activity and it is unclear how they would be predicted for a task with significant activity.

Muscle Name	Mean RMS Error % \pm Standard of Deviation	Min. / Max RMS Error %
M1 - Serratus Anterior	7.06 \pm 4.98	1.24 / 21.81
M2 - Anterior Deltoid	9.00 \pm 3.54	4.26 / 21.27
M3 - Posterior Deltoid	5.95 \pm 3.90	1.17 / 18.66
M4 - Pectoralis Major	8.33 \pm 3.65	3.91 / 21.90
M5 - Latissimus Dorsi	8.19 \pm 3.51	3.33 / 23.03
M6 - Teres Major	6.25 \pm 3.69	2.36 / 22.95
M7 - Biceps Brachii	4.49 \pm 2.59	2.34 / 18.63
M8 – Brachialis	6.25 \pm 2.24	2.34 / 14.75
M9 – Brachioradialis	4.16 \pm 1.82	1.83 / 13.66
M10 - Triceps Brachii	7.75 \pm 3.68	2.18 / 18.13
M11 - Extensor Carpi Radialis Longus	3.74 \pm 1.87	1.82 / 13.84
M12 - Flexor Carpi Radialis	2.10 \pm 1.22	1.03 / 8.55
Overall	6.11 \pm 3.06	1.03 / 23.03

Table 3: Synopsis of muscle RMS errors collapsed over all tasks and trials. Values shown in percent.

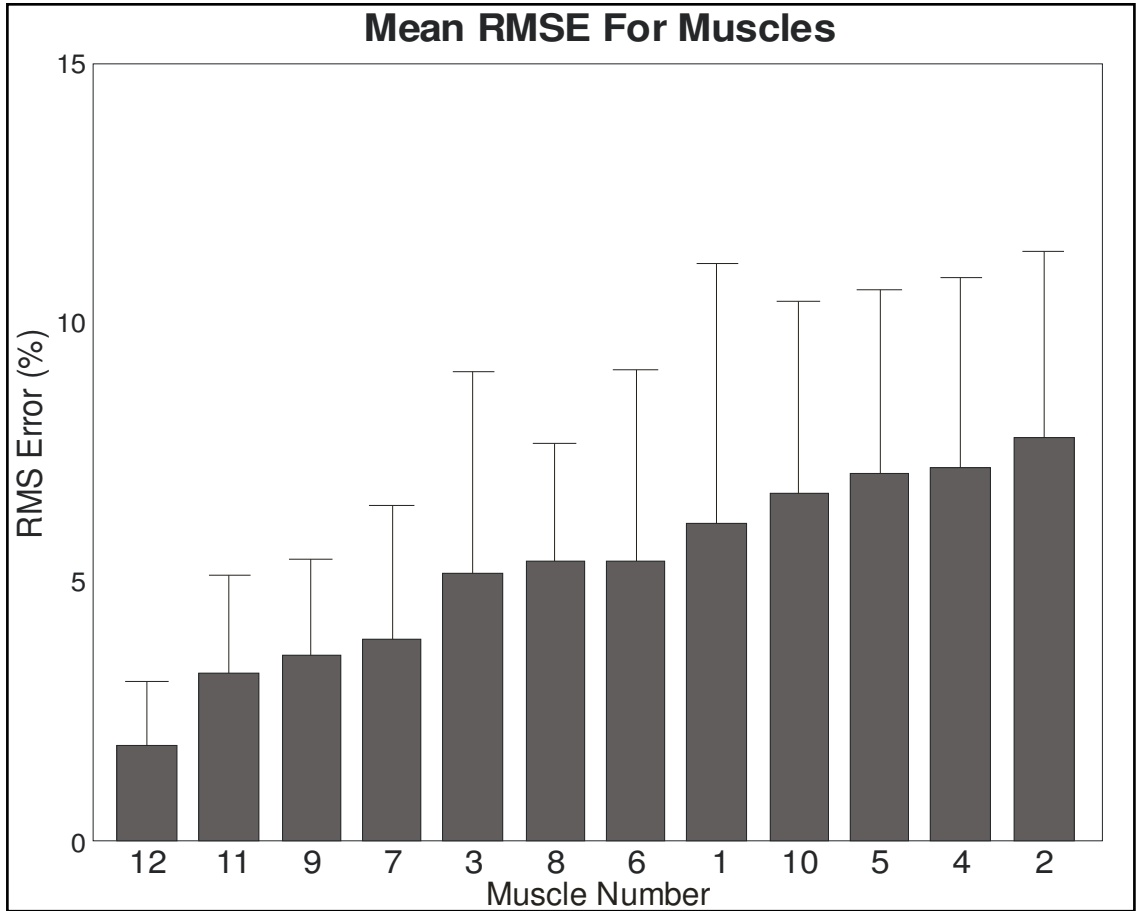


Figure 19: Muscles ranked in order of ascending RMS error.

Chapter 6: Discussion

Previously, Seifert and Fuglevand [18] showed good correspondence between desired muscle activity and predicted muscle activity resulting in 12.1% RMS error across three muscles and five movements. Additionally, for this amount of RMS error, they were able to also show that a frequency modulated pulse train derived from the predicted EMG and then delivered to the muscles as a stimulus pattern evoked a movement response which closely matched the desired with RMS errors ranging from 21.8% to 23.8% across all movements, subjects, tasks and trials. Overall, these errors were modest and the evoked movements corresponded well to the desired movements.

This thesis shows the successful extension of the work done previously by Seifert and Fuglevand [18] by demonstrating that Bayes' theorem can be used to estimate the muscle activity during natural complex movements for the many muscles associated with movements of a human limb. Furthermore, this estimation was achieved with a high degree of accuracy with mean RMS errors around 6.1%. The improvement over the results from Seifert and Fuglevand is most likely due to the extended duration and the less constrained movement of task 1, the training task used to establish the probability density functions.

Though introduced as an alternative method for mapping kinematic signals to muscle activity, the use of artificial neural networks has not been directly applied to the problem of estimating muscle activity from kinematic information. However, the inverse problem of mapping muscle activity signals to kinematic values has been lightly investigated. Some results are presented because, though these results are not directly comparable to the results of the experiment presented in this thesis, the estimation process described in this thesis is reversible so that kinematic values could be predicted given muscle activity levels and it is expected that the RMS errors would be similar, about 6.1%. Au and Kirsch [1] reported RMS errors of 14% - 19% in a study where artificial neural networks were used to predict kinematic information from muscle activity signals recorded from six muscles during three movement types. A simplified but parallel problem was considered by Massone and Bizzi [13] wherein a neural network was used to predict the driving signals to a mechanical arm loosely based on a simplified model of the human arm. They reported good success in the ability of the artificial neural network to drive the mechanical arm to a desired end point position. Cheron and Dray [4] also showed that an artificial neural network could map EMG derived signals to 2-D kinematic values. They showed good success though no error quantity was given.

6.1 For Future Study

There were a few items which did not receive treatment in this thesis which are germane to the technique presented and/or the specific, proposed application. Each are presented in brief summary.

6.2 Dimensionality

This study only included two-dimensional kinematic data. However, real arm movements take place in three dimensions. It should be understood that for movements within a single plane, some muscles are not used except in a stabilizing role. It is expected that movements in three dimensions would give rise to interesting muscle activity on some of those muscles which, for this study, served only to stabilize the arm. Based on the predictions for muscles which contributed significantly during the two dimensional movements, it is expected that given three dimensional position data the predictions for those muscles which would become more active could be predicted with similar results to the predictions of muscles active during movements confined to a single plane.

6.3 Independence Assumption

This study assumes that the activity of each muscle is independent of the activity in all the other measured muscles. It is highly unlikely that this is the case. The following modification to the Bayes' process described by this thesis might cover the case of non-independence between muscles. In addition to finding the joint probability density functions between each muscle and each kinematic parameter, the joint probability density functions between each muscle and each other muscle might also be calculated. Then in an iterative approach, the predicted value for each muscle could be determined. The initial guess of EMG for each muscle would assume independence as was done in this study. Once that predicted value was found, the prediction for each muscle could be recalculated, adding in the predicted values of all other muscles as additional dependencies. Then, the process could be repeated until some criteria for the amount of change allowed was reached or for a specified number of iterations. One of three possible outcomes would result. The predicted EMG values would enter a limit cycle, converge or diverge.

6.4 Kinematic Parameters

The results presented by this thesis are based solely on the positional kinematic parameters. However, the additional parameters of velocity and acceleration were also investigated. It was found that, contrary to expectation, additional kinematic parameters

which provide some history information like velocity and acceleration, did not improve the prediction. They actually degraded the prediction and resulted in higher RMS errors. This might be due to the amplification of noise during the differentiation process, the time scale of the velocity and acceleration data, or, this effect could be simply because positions translate into muscle activity better than velocities and accelerations so that the introduction of velocity or acceleration into the equation was equivalent to the introduction of greater error. These results were not presented because the cause of the deteriorated results is still not clear. If noise amplification due to differentiation caused the degraded performance, then appropriate filtering might greatly improve performance. If the time scale was resulting in degraded performance, the average velocity or acceleration over some longer period, e.g. $\frac{1}{2}$ second or 1 second, could be used.

6.5 Implications for Functional Electrical Stimulation (FES)

In any FES system, muscles are stimulated by electrodes delivering electric pulses. The predictor described in this thesis provides an estimate of the global muscle activity. However, an estimate of muscle activity could be used as a controller in an FES system using a transformation from predicted muscle activity to a frequency modulated pulse train which could be delivered to muscles as done in Seifert and Fuglevand [18].

Because a user of an FES system cannot produce the EMG and kinematic data needed to form a training set for the Bayesian estimation technique presented here, it would be important to determine how the system would work when the set of training data came from a subject other than the one using the system. Based on the work of Seifert and Fuglevand [18], it is expected that using different subjects for training and for implementation would not affect the system too adversely, i.e. the predictor should still work with minimal worsening of predictions. However, if problems arose between subjects or if the joint densities changed with time, an adaptive approach could be employed wherein the density functions would be continually updated during use. For example, this could be done by simply forming the required densities of a batch of data, adding it to the existing densities and renormalizing. This process reinforces correct correlations and minimizes the effect of incorrect correlations.

6.6 Summary

The results presented in this thesis could be the key element in connecting two research camps that are currently working to develop neuroprosthetic systems to restore movement in paralyzed individuals. On one side, many researchers have worked extensively on cortical control of robotic devices. Their work has focused on generating trajectory information by interpreting the neural activity recorded from the brain. They have avoided the problem associated with the control of real muscles by restricting their

application to the control of robotic arms. On the other side, many researchers have worked for years to restore some use of the natural limb through functional electrical stimulation. They have been limited by the severe shortcomings in the control of these systems and have settled for using joysticks and preprogrammed movements. This project has the potential to combine the technology of both parties and produce a truly viable neuroprosthetic solution.

Appendix A – Atlas of Electromyography

This appendix contains diagrams of the locations of EMG recording sites for each muscle. All illustrations in this appendix were taken from [12].

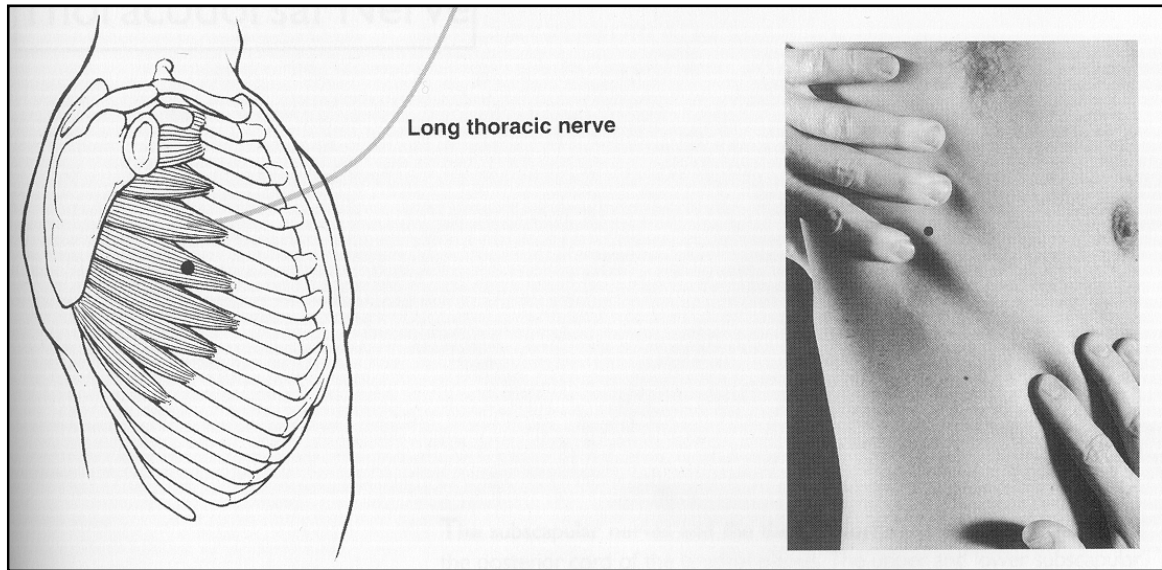


Figure 20: The location of M1, serratus anterior. The black dot marks the recording site.

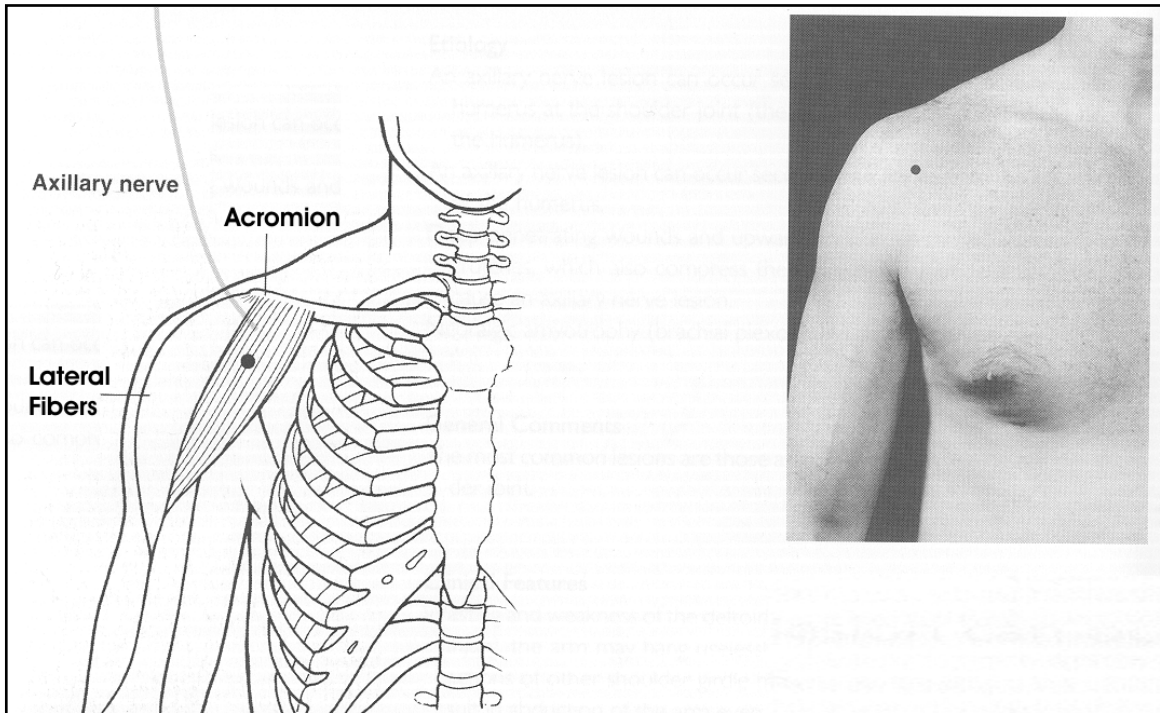


Figure 21: The location of M2, anterior deltoid. The black dot marks the recording site.

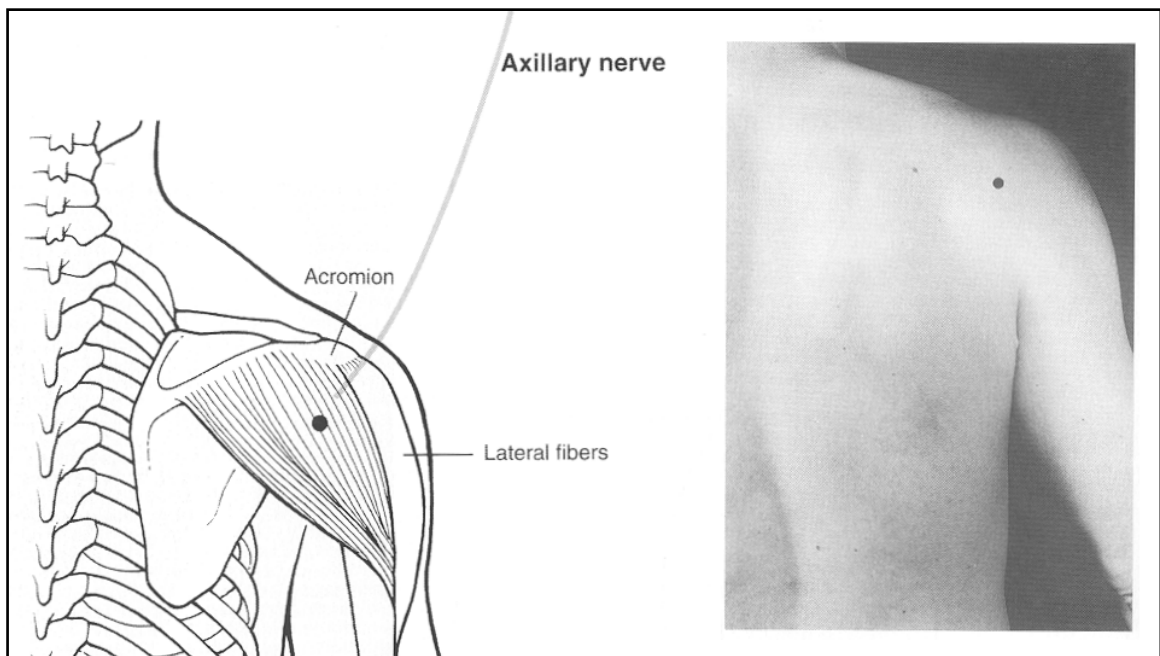


Figure 22: The location of M3, posterior deltoid. The black dot marks the recording site.

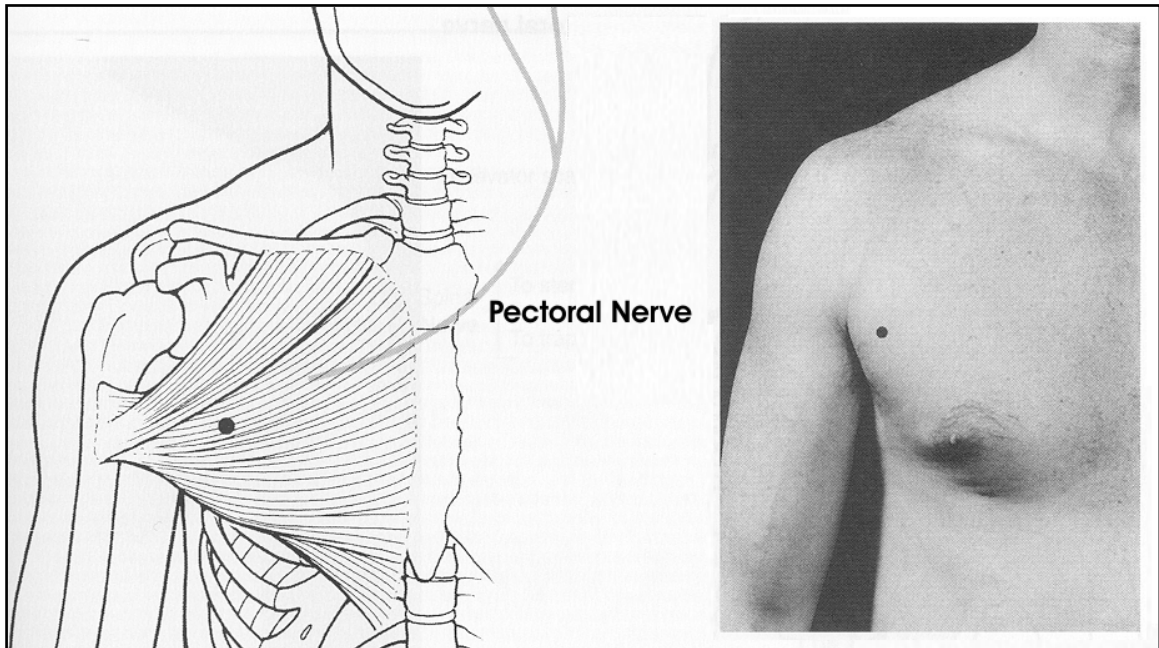


Figure 23: The location of M4, pectoralis major. The black dot marks the recording site.

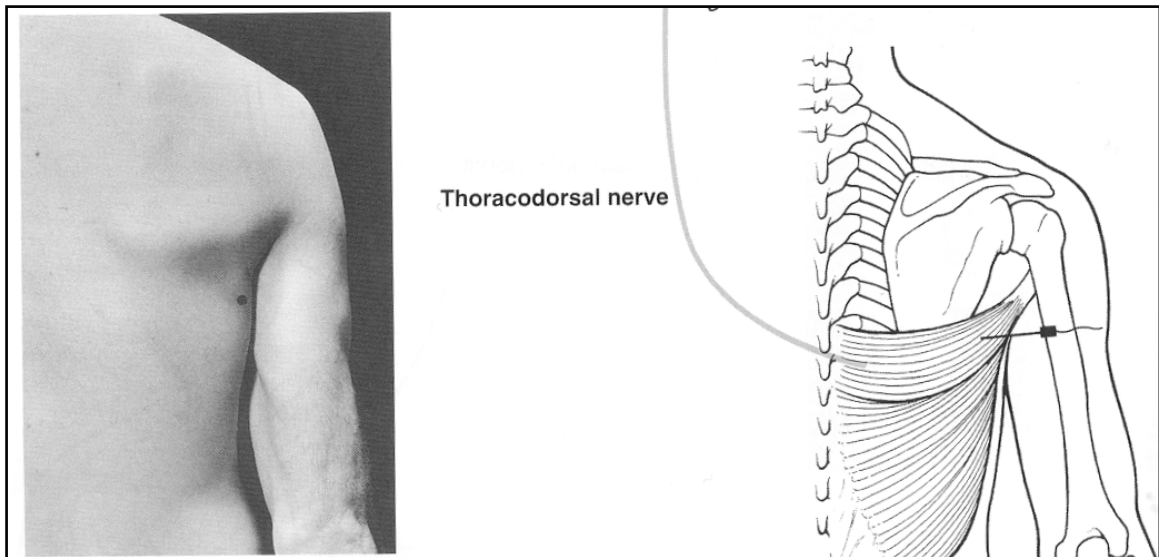


Figure 24: The location of M5, latissimus dorsi. The black dot marks the recording site.

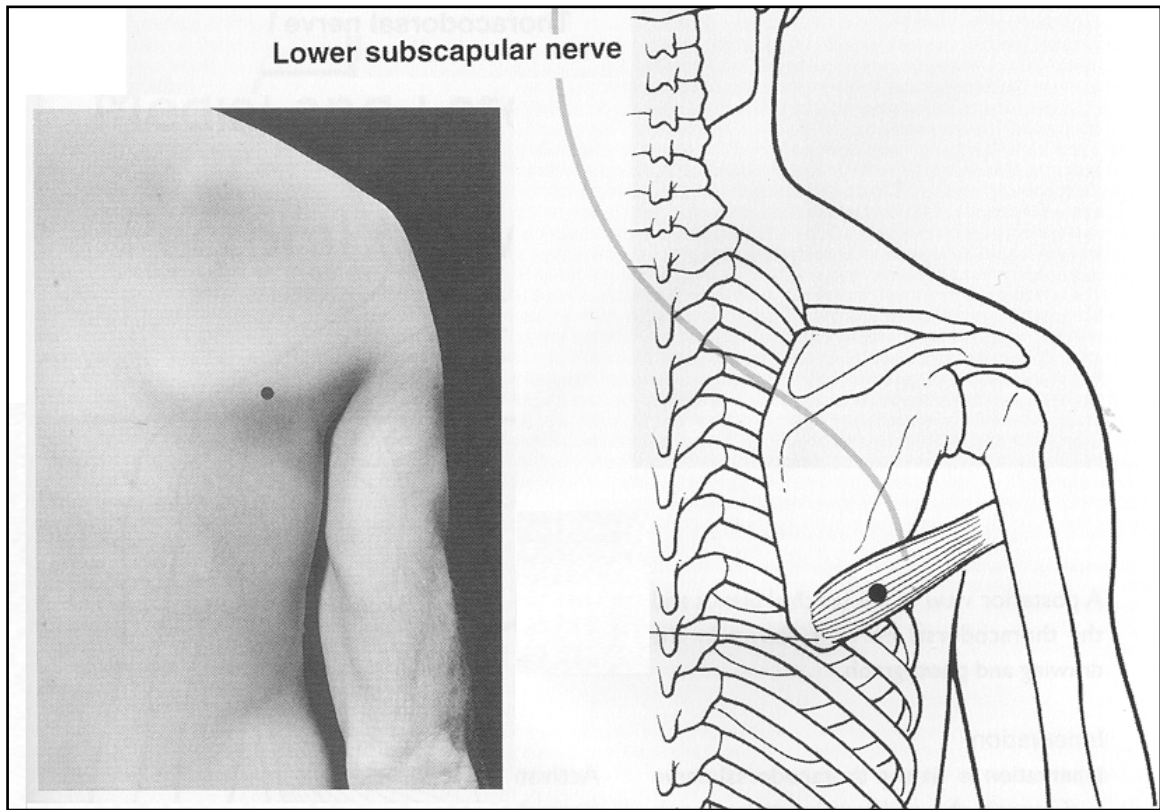


Figure 25: The location of M6, teres major. The black dot marks the recording site.

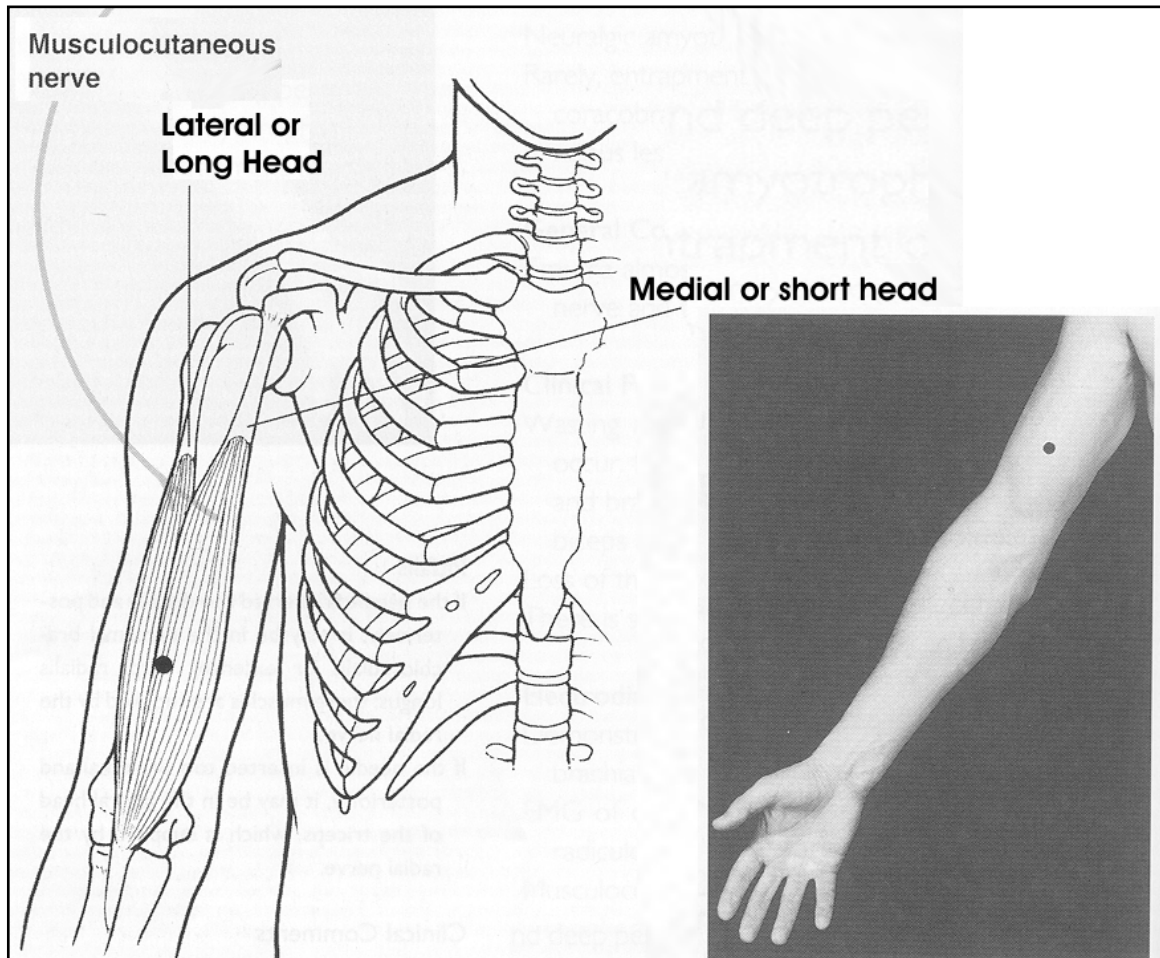


Figure 26: The location of M7, biceps brachii. The black dot marks the recording site.

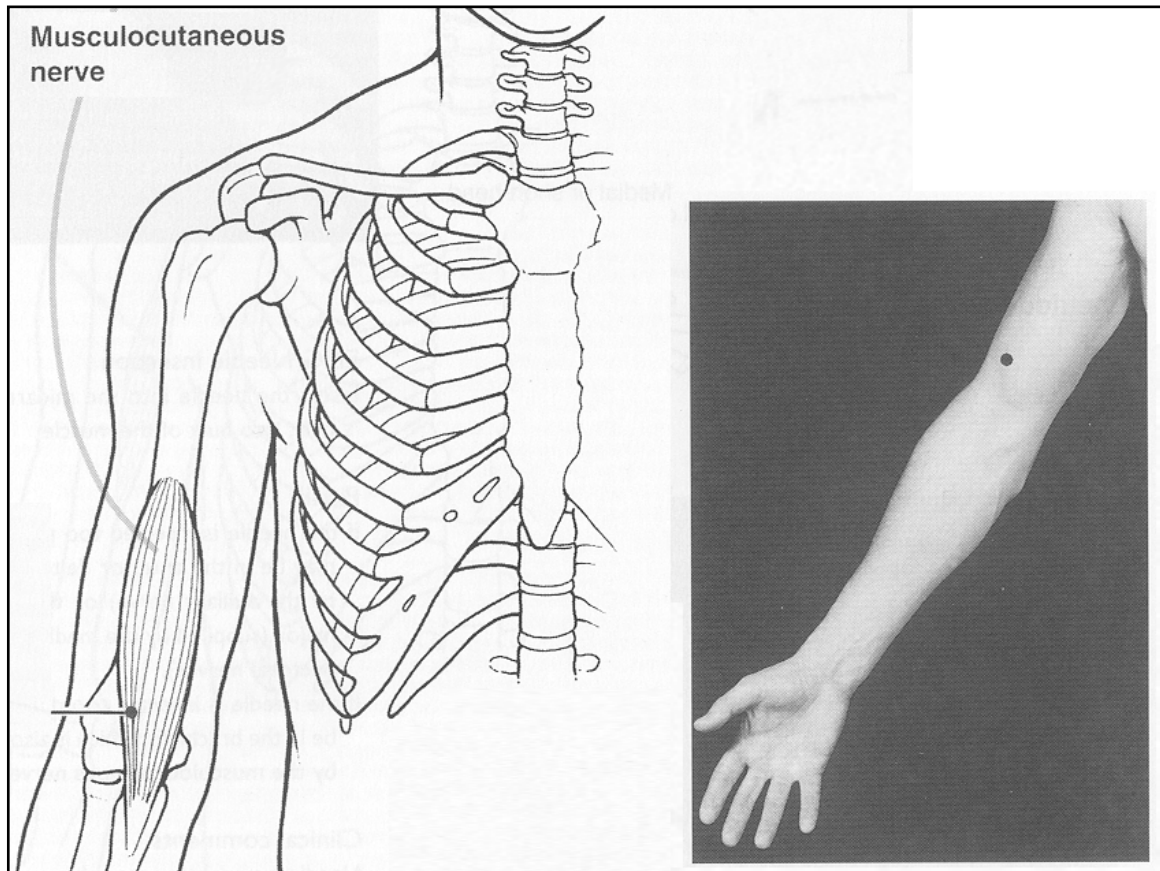


Figure 27: The location of M8, brachialis. The black dot marks the recording site.

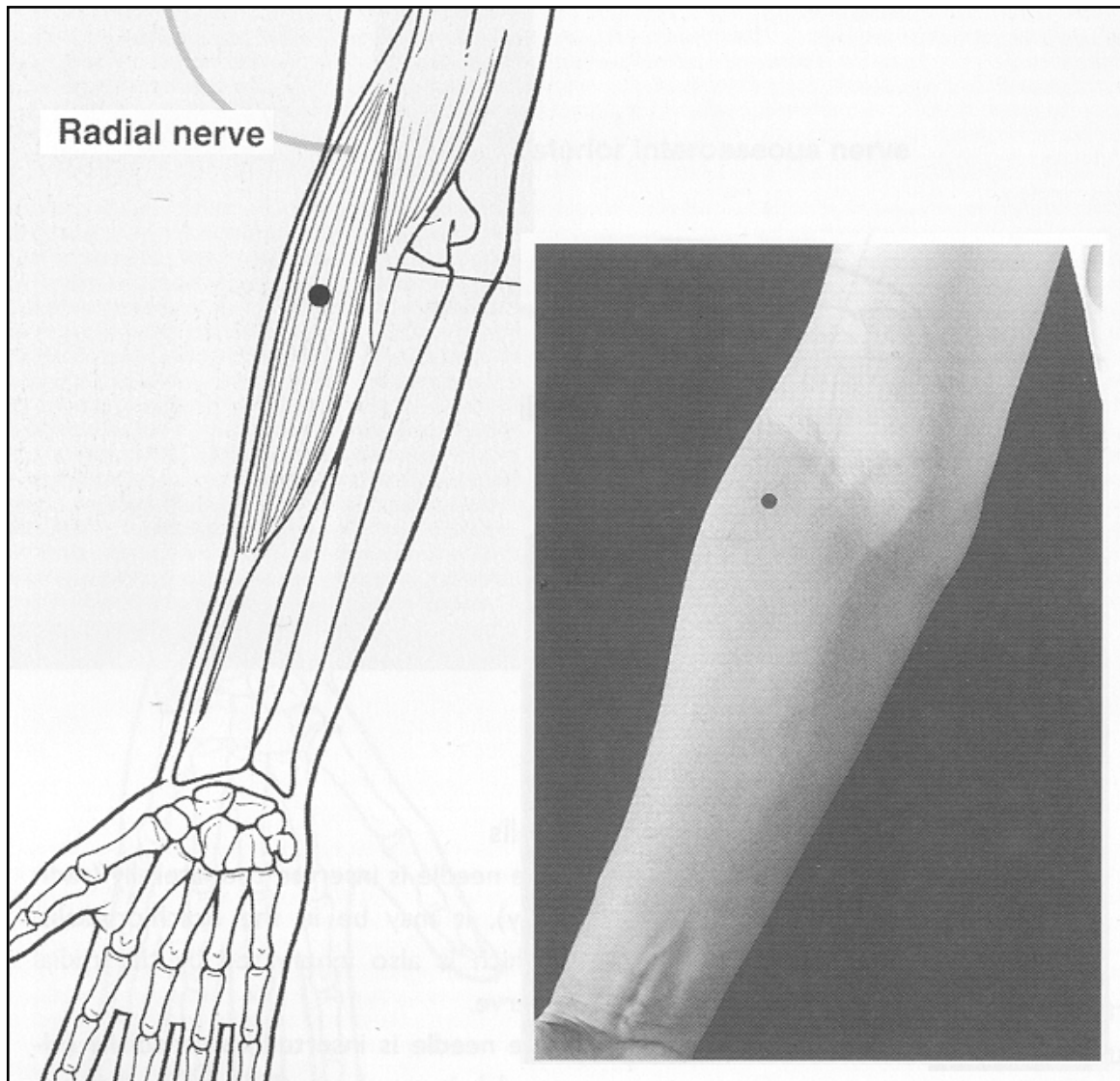


Figure 28: The location of M9, brachioradialis. The black dot marks the recording site.

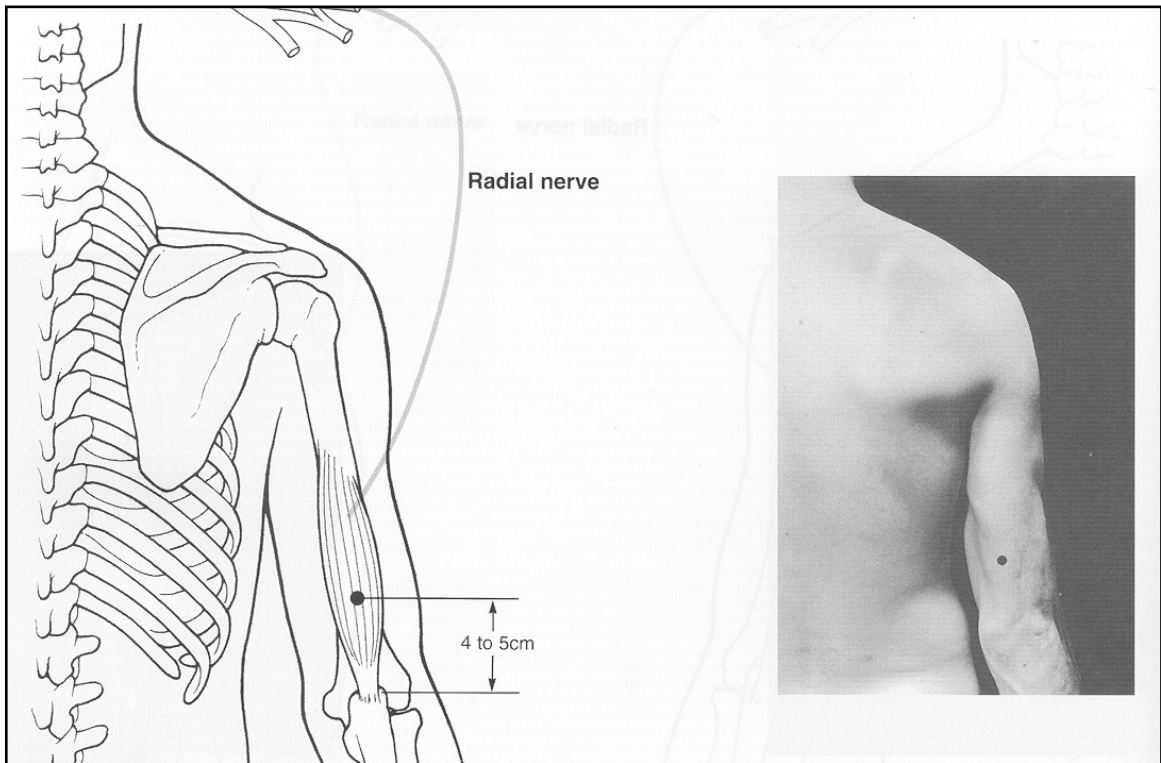


Figure 29: The location of M10, triceps. The black dot marks the recording site.

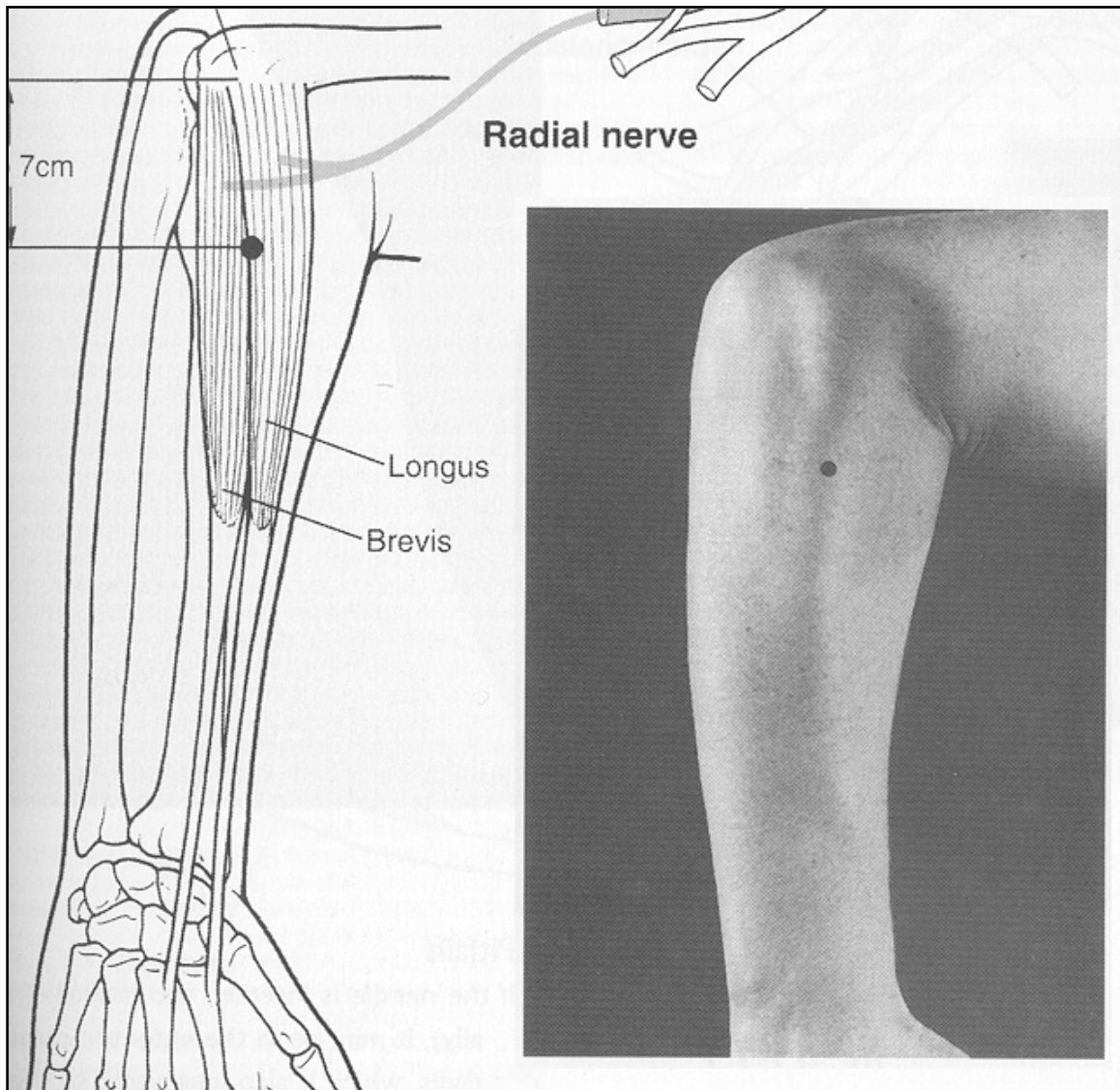


Figure 30: The location of M11, extensor carpi radialis. The black dot marks the recording site.

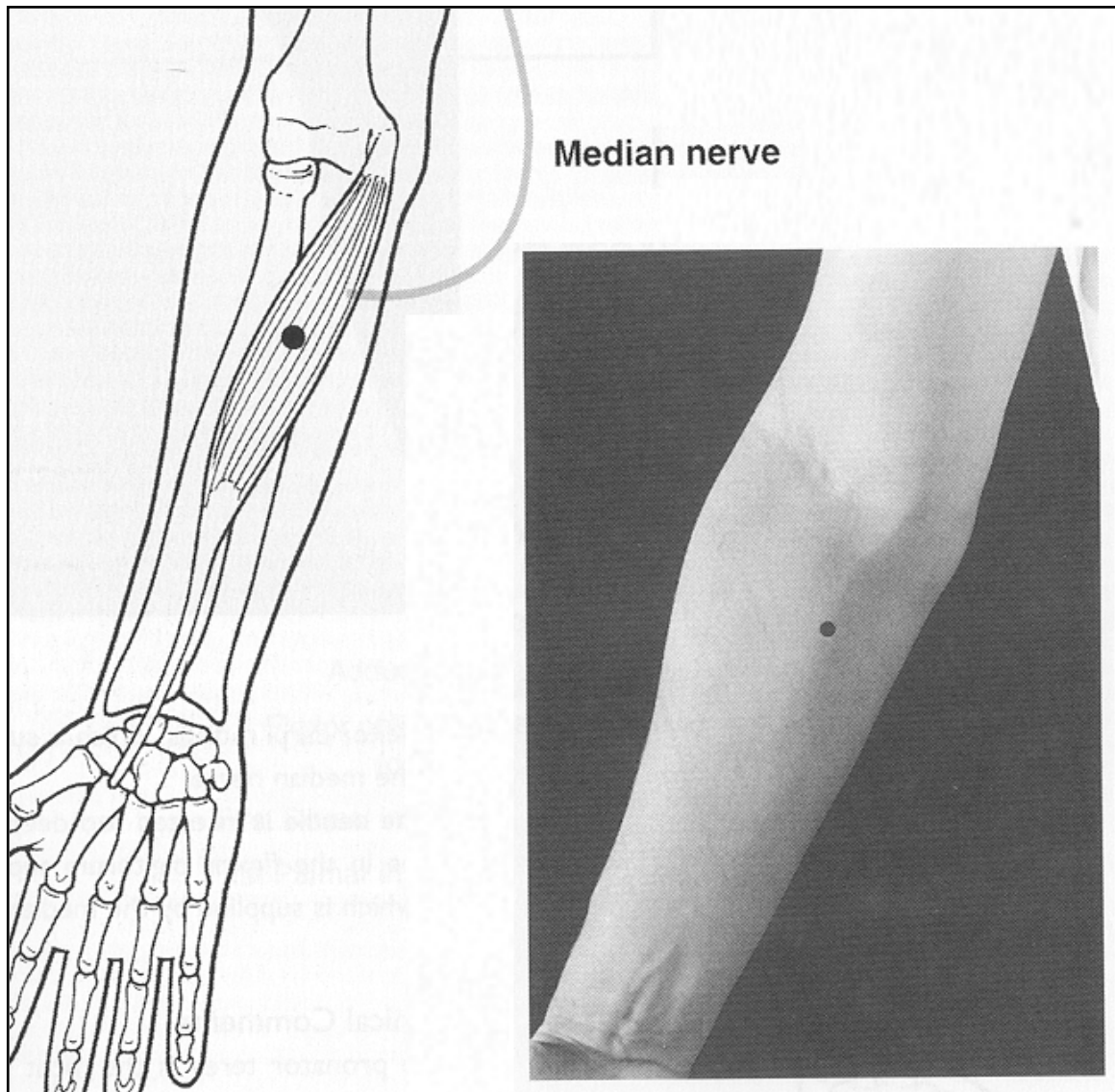


Figure 31: The location of M12, flexor carpi radialis. The black dot marks the recording site.

References

- [1] Au, A.T.C. and Kirsch, R.F., "EMG-Based Prediction of Shoulder and Elbow Kinematics in Able-Bodied and Spinal Cord Injured Individuals," *I.E.E.E. Transactions on Rehabilitation Engineering*, vol. 8, no. 4, pp. 471-480, Dec. 2000.
- [2] Black, T.C., Thompson, W.J., "Bayesian Data Analysis," *Computing in Science and Engineering*, vol. 3, iss. 4, pp. 86-91, July/Aug. 2001.
- [3] Blinowska, A., Chatellier, G., Bernier, J., and Lavril, M., "Bayesian Statistics as Applied to Hypertension Diagnosis," *I.E.E.E. Transactions on Biomedical Engineering*, vol. 38, issue 7, pp. 699-706, Jul. 1991.
- [4] Cheron, G., Draye, J.P., Bourgeois, M. and Libert, G., "A Dynamic Neural Network Identification of Electromyography and Arm Trajectory Relationship during Complex Movements," *I.E.E.E. Transaction on Biomedical Engineering*, vol 43, no. 5, pp. 552-558, May 1996.
- [5] Clancy, E.A., Morin, E.L., Merletti, R., "Sampling, Noise-Reduction and Amplitude Estimation Issues in Surface Electromyography," *Journal of Electromyography and Kinesiology* vol 12, pp. 1-16, Sept. 2001.
- [6] Deadwyler, S.A., Hampson, R.E., "The Significance of Neural Ensemble Codes During Behavior and Cognition," *Annual Review Neuroscience*, vol. 20, pp. 217-244, 1997.
- [7] Graupe, D. Kordylewski, H., "Artificial Neural Network Control of FES in Paraplegics for Patient Responsive Ambulation," *I.E.E.E. Transactions on Biomedical Engineering*, vol. 42, no. 7, pp. 699-707, July 1995.
- [8] Hoshimiya, N. Naito, A., Yajima, M., Handa, Y., "A Multichannel FES System for the Restoration of Motor Functions in High Spinal Cord Injury Patients: A Respiration-Controlled System for Multijoint Upper Extremity," *I.E.E.E. Transactions on Biomedical Engineering*, vol. 36, no. 7, pp. 754-760, July 1989.

- [9] Huo, Q. and Lee, C.H., "A Bayesian Predictive Classification Approach to Robust Speech Recognition," *I.E.E.E. Transactions on Speech and Audio Processing*, vol. 8, issue 2, pp. 200-204, March 2000.
- [10] Kamen, G., Caldwell, G., "Physiology and Interpretation of the Electromyogram," *Journal of Clinical Neurophysiology*, vol. 13, no. 5, pp. 366-384, 1996.
- [11] Kang, D. Luo, R.C., Hashimoto, H., Harashima, F., "Position Estimation for Mobile Robot Using Sensor Fusion," *Multisensor Fusion and Integration for Intelligent Systems, 1994. IEEE International Conference on MFI '94.*, iss., 2-5, pp. 647-652, Oct 1994.
- [12] Leis, A.A., Trapani, V.C., *Atlas of Electromyography*, New York: Oxford University Press, Inc., 2000, pp. 21-93.
- [13] Massone, L. and Bizzi, E., "A Neural Network Model for Limb Trajectory Formation," *Biological Cybernetics*, vol. 61, pp. 417-425, 1989.
- [14] Nicolelis, M., *Journal of Neurosurgery*, (forthcoming), July 2004.
- [15] Peckham, P.H., Keith, M.W., et. al., "Efficacy of an Implanted Neuroprosthesis for Restoring Hand Grasp in Tetraplegia: A Multicenter Study," *Archives of Physical Medicine and Rehabilitation*, vol. 82, pp. 1380-1388, Oct. 2001.
- [16] Peckham, P.H., Kilgore, K.L., et. al., "An Advanced Neuroprosthesis for Restoration of Hand and Upper Arm Control Using an Implantable Controller," *The Journal of Hand Surgery*, vol. 27, pp. 265-276, 2002.
- [17] Putnam, C.A., "A Segment Interaction Analysis of Proximal-to-Distal Sequential Segment Motion Patterns," *Medicine & Science in Sports & Exercise*, vol. 23, no. 1, pp. 130-144, Jan. 1991.
- [18] Seifert, H.M. and Fuglevand, A.J., "Restoration of Movement Using Functional Electrical Stimulation and Bayes' Theorem," *The journal of Neuroscience*, vol. 22, pp. 9465-9474, Nov. 2002.

- [19] Sennels, S., Biering-Sorensen, F., Andersen, O.T., Hansen, S.D., "Functional Neuromuscular Stimulation Controlled by Surface Electromyographic Signals Produced by Volitional Activation of Same Muscle: Adaptive Removal of the Muscle Response from the Recorded EMG-Signal," *I.E.E.E. Transactions on Rehabilitation Engineering*, vol. 5, no. 2, pp. 195-197, June 1997.
- [20] Soechting, J.F., Flanders, M., "Evaluating an Integrated Musculoskeletal Model of the Human Arm," *Journal of Biomechanical Engineering*, vol. 119, pp 93-102, Feb. 1997.
- [21] Stansfield, B.W., Nicol, A.C., Paul, J.P., Kelly, I.G., Graichen, F., Bergmann, G., "Direct Comparison of Calculated Hip Joint Contact Forces with Those Measured Using Instrumented Implants. An Evaluation of a Three-Dimensional Mathematical Model of the Lower Limb," *Journal of Biomechanics*, vol. 36, pp. 929-936, 2003.
- [22] Taylor, D.M., Tillery, S.I.H., Schwartz, A.B, "Direct Cortical Control of 3D Neuroprosthetic Devices," *Science*, vol. 296, pp. 1829-1832, June 2002.
- [23] Wessberg, J., et. al., "Real-Time Prediction of Hand Trajectory by Ensembles of Cortical Neurons in Primates," *Nature*, vol. 408, pp. 361-365, November 2000.
- [24] Winter, D.A., *Biomechanics of Human Movement*, New York: John Wiley & Sons, 1979, pp. 32-39, 139-145.
- [25] Wolpert, D.M. and Ghahramani, Z., "Computational Principles of Movement Neuroscience," *Nature Neuroscience Supplement*, vol. 3, pp. 1212-1217, Nov. 2000.
- [26] Zhang, K., Ginzburg, I., McNaughton, B.L. and Sejnowski, T.J., "Interpreting Neuronal Population Activity by Reconstruction: Unified Framework With Application to Hippocampal Place Cells," *Journal of Neurophysiology*, vol. 79, pp. 1017-1044, Aug. 1998.